1

The Moving Bed Fuel Reactor Process

Andrew Tong, Mandar V. Kathe, Dawei Wang, and Liang-Shih Fan

The Ohio State University, Department of Chemical Engineering, 151 W. Woodruff Ave, Columbus, OH 43210, USA

1.1 Introduction

Chemical looping refers to the use of a chemical intermediate in a reaction-regeneration cycle to decompose one target reaction into two or more sub-reactions. The decomposition of the target reaction with a reactive chemical intermediate can decrease the process irreversibility, and, thus, increase the recoverable work from the system yielding a higher exergy efficiency. Further, when one or more of the reactant feedstocks consist of an inert substrate, the chemical looping reaction pathway is designed to prevent the direct contact of the inert with the desired product, minimizing the product purification steps required [1–3]. In 1987, Ishida et al. was the first publication to use the term, "chemical looping," referring to the use of a metal oxide as the chemical intermediate to perform oxidation–reduction reaction cycles for power generation applications [4]. However, Bergmann's invention of a calcium carbide production process using manganese oxide redox reaction cycles with carbonaceous fuels suggests that the chemical looping concept was in development as early as 1897 [5]. Table 1.1 summarizes the early developments of chemical looping processes in the twentieth century [6–9, 12–21]. Though several achieved pilot scale demonstration, no early chemical looping processes were able to achieve widespread commercial realization due to limitations in the oxygen carrier reactivity, recyclability, and attrition resistance and the reactor design for maintaining, continuous high product yield.

With growing concerns of greenhouse gas emissions, a renewed effort in developing chemical looping processes occurred at the start of the twenty-first century as reflected in the exponential growth of research publications [1]. As of 2012, over 6000 cumulative hours of operation of chemical looping processes for power generation with CO_2 capture have been demonstrated over fuel processing capacities ranging from 300 W_{th} to 3 MW_{th} [22]. Nearly all chemical looping processes at the pilot scale demonstration have adopted a fluidized bed reactor design for the conversion of the fuel source to CO_2/H_2O, or the fuel reactor [23]. Recent developers are investigating fixed bed reactors to perform

Handbook of Chemical Looping Technology, First Edition. Edited by Ronald W. Breault.

Table 1.1 Summary of early chemical looping process development.

Process/ developer	Lane [6–11]	Lewis and Gilliland	HYGAS	CO_2 acceptor	HyPr-Ring
Year developed	1910s	1950s	1970s	1960s–1970s	1990s
Feedstock	Syngas	Solid fuel	Syngas	Solid fuel	Solid fuel
Products	H_2	CO_2	H_2	H_2 rich syngas	H_2
Chemical intermediate	Fe_3O_4—Fe	CuO—Cu_2O or Fe_2O_3—Fe_3O_4	Fe_3O_4—Fe	$CaCO_3$—CaO	$CaCO_3$—CaO/ $Ca(OH)_2$
	ARCO GTG	**DuPont**	**Otsuka**	**Solar water splitting**	**Steinfeld**
Year	1980s	1990s	1990s	1980s	1990s
Feedstock	CH_4	C_4H_{10}	CH_4	H_2O	CH_4, iron ore
Products	C_2H_4	$C_4H_2O_3$	Syngas	H_2, O_2	Syngas, iron
Chemical intermediate	Supported Mn	VPO	Supported CeO_2	ZnO—Zn or Fe_3O_4—FeO/Fe	Fe_3O_4—Fe

the cyclic oxidation–reduction reactions with chemical looping oxygen carriers for power generation and chemical production applications [24–27]. Alternatively, chemical looping processes utilizing a moving bed fuel reactor are under development for full and partial fuel conversion for CO_2 capture/power generation and syngas production, respectively [23, 28, 29]. This chapter describes the use of moving reactors for chemical looping processes with specific application to syngas and power production with CO_2 capture using metal oxide materials as oxygen carrier chemical intermediates. Two modes of moving bed operation are discussed and their application for full and partial fuel oxidation. Reactor thermodynamic modeling combined with experimental results are provided.

1.2 Modes of Moving Bed Fuel Reactor Operation

As illustrated in Figure 1.1, the moving bed fuel reactor can be operated in the counter-current or co-current mode based on the gas–solid flow contact pattern with Fe-based oxygen carrier as the exemplary chemical intermediate [1]. The counter-current moving bed fuel reactor in Figure 1.1a achieves a high oxygen carrier conversion while maintaining high CO_2 product purity. The oxygen carrier conversion, as defined in Eq. (1.1), is the mass ratio of the amount of oxygen used from the oxygen carrier exiting the fuel reactor relative its maximum available oxygen.

$$X_O = \frac{m_{ox} - m_{red}}{m_{ox} - m_{red}^{full}} \times 100\% \tag{1.1}$$

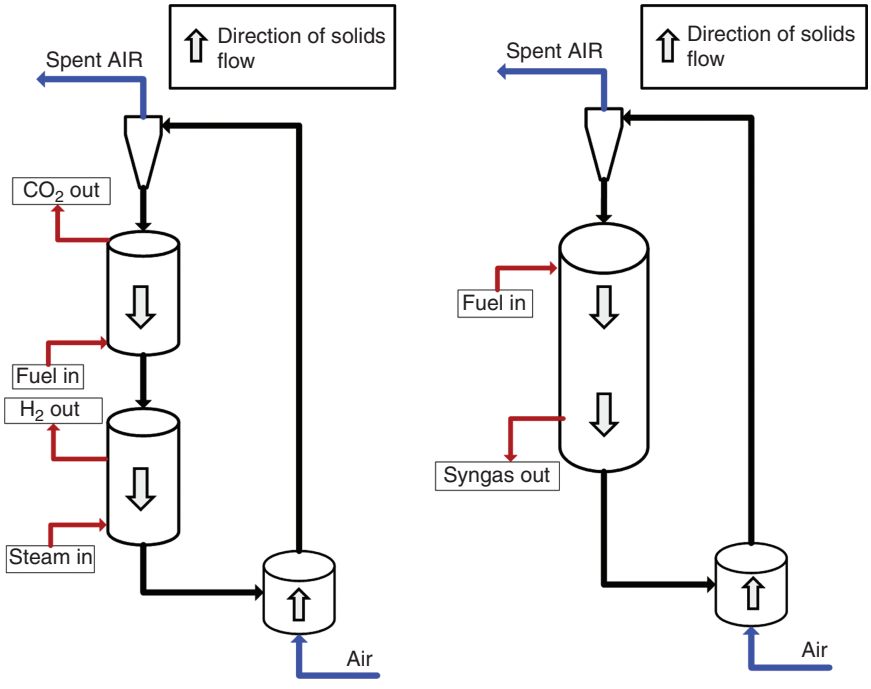

Figure 1.1 Conceptual design of a moving bed chemical looping processes with a counter-current (a) and co-current (b) fuel reactor for full fuel conversion to CO_2/H_2O and for fuel gasification/reforming to syngas, respectively.

where m_{ox} and m_{red} refer to the mass of the fully oxidized and the reduced sample at the outlet of the fuel reactor, respectively, and m_{red}^{full} refers to the mass of the sample at the fully reduced state (e.g. metallic iron for Fe-based oxygen carriers).

Figure 1.1b shows the co-current moving bed fuel reactor for partial oxidation of the solid or gaseous fuel source to syngas. The co-current process allows for accurate control of the oxygen carrier and fuel residence times, ratios, and distribution to maintain continuous high purity syngas. The present section discusses the advantages of each mode of the moving bed reactor operation and considers several applications for solid and gaseous fuel conversion for each.

1.2.1 Counter-Current Moving Bed Fuel Reactor:

In a counter-current moving bed operation of chemical looping process, the gas species in the fuel reactor travel the opposite direction relative to the solids flow. Further, the gas species operate below the minimum superficial gas velocity and, thus, travel only through the interstitial spaces of the packed moving bed of oxygen carrier solids. For full fuel conversion, the counter-current moving bed design is capable of maintaining high CO_2 purities and reducing the oxygen carrier to a low oxidation state, ideal for metal oxides with multiple oxidation states such as iron [30, 31]. Figure 1.2 is an example of operation lines for moving bed chemical looping fuel reactor and steam reactor. The figure illustrates

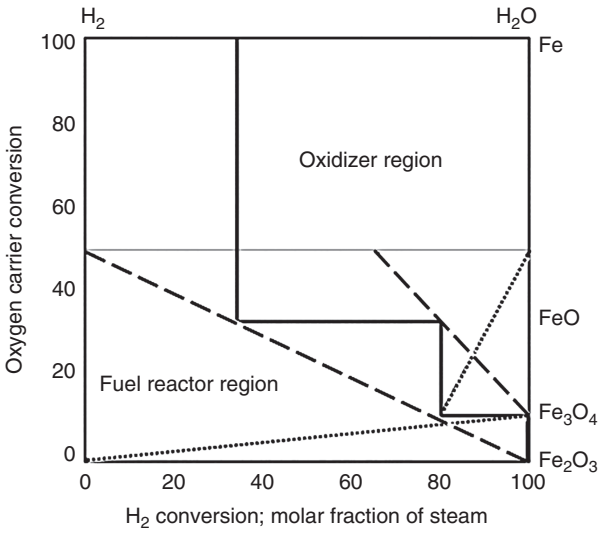

Figure 1.2 Operation lines for moving bed chemical looping fuel reactor and steam reactor.

the phase equilibrium of a Fe-based oxygen carrier particle at varying partial pressures (i.e. conversions) of the reducing gas at 850 °C. In the figure, the solid line represents the phase equilibrium of iron. The dashed line in the fuel reactor region represents the counter-current reactor operation while the dotted line represents the fluidized bed/co-current operation. The slope of the moving bed and fluidized bed operating lines are determined based on the oxygen balance between the oxygen carrier and the gas species. In the case of fluidized bed operation with iron-based oxygen carrier, the maximum oxygen carrier conversion achievable is 11% (i.e. reduction from Fe_2O_3 to Fe_3O_4), as a higher oxygen carrier conversion will result in a decrease in product purity from the fuel reactor. Further, the high extent of reduction of the iron oxide oxygen carrier achieved in the counter-current fuel reactor allows for thermodynamically favorable reaction of Fe/FeO with H_2O to produce H_2 via the steam–iron reaction. High purity H_2 production from a third reactor, i.e. the steam reactor, increases the product flexibility of the processes and can serve as an advanced approach for H_2 production with minimal process operations for product separation compared to traditional steam–methane reforming (SMR).

Figure 1.3 illustrates the design of the counter-current fuel reactor for solid fuel conversion to CO_2. Here, the fuel reactor is divided into two sections [32–34]. Once the solid fuel is introduced to the high temperature fuel reactor, it devolatilizes and the solid char species travel downward co-currently with the flow of oxygen carrier solids into the char gasification section. The volatiles travel upward counter-currently with the flow of the oxygen carrier. In the lower bed, the solid char is gasified using an enhancer gas consisting of CO_2 and/or H_2O recycled from the flue gas produced from the fuel reactor. The gasified char and volatile matter are polished to CO_2 and H_2O in the upper reactor bed. The

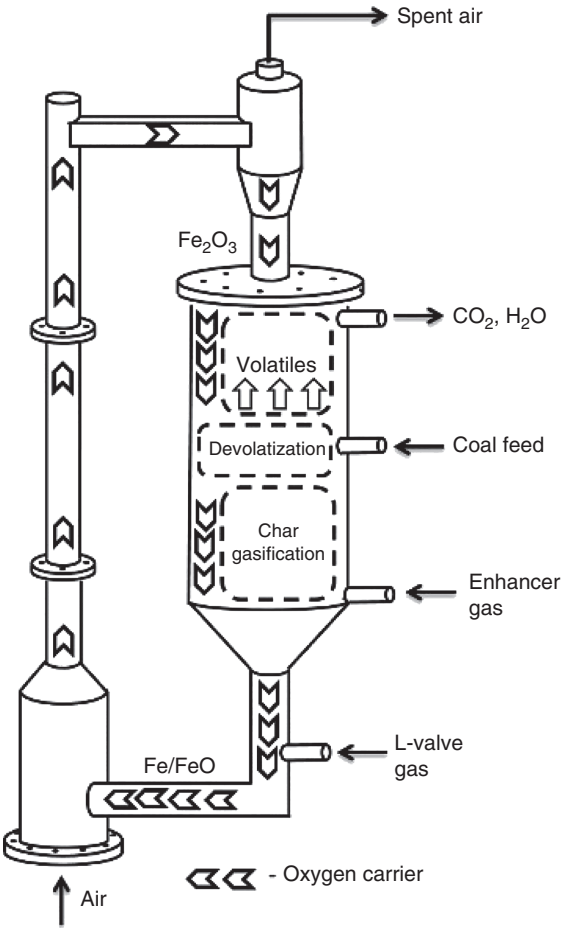

Figure 1.3 Conceptual design of the counter-current moving bed fuel reactor for solid fuel conversion to CO_2/H_2O.

packed moving bed reactor is designed to provide sufficient residence time for the solid fuel gasification and the fully oxidized Fe_2O_3 oxygen carrier entering the top section 1 reactor ensures CO_2 purity exiting the process is nearly 100% after H_2O is condensed out. No additional downstream conditioning equipment and/or molecular oxygen is required to fully oxide the solid fuel to CO_2, which translates to high process efficiency and reduced process capital costs. At Ohio State University (OSU), two chemical looping processes using a counter-current moving bed fuel reactor have been scaled to pilot plant demonstration for the conversion of gaseous fuels (the syngas chemical looping (SCL) process) and solid fuels (the coal direct chemical looping (CDCL), process) to H_2 and heat, respectively, with CO_2 capture. The SCL process is promising technology capable of reducing the H_2 separation costs compared to traditional coal gasification and the SMR process with natural gas. The CDCL process is an advance oxy-combustion technology for CO_2 capture from coal. Further details on the pilot plant developments are discussed in Section 1.4.

1.2.2 Co-current Moving Bed Fuel Reactor

In the co-current moving bed fuel reactor operation, the gas species travel in the same directions as the solid flow [23]. The gas flow rate is operated below the minimum fluidization velocity to ensure uniform gas velocity profile across the fuel reactor is achieved for precise and independent control of the gas and solid residence times. Co-current moving bed fuel reactors are generally used for the partial oxidation of carbonaceous fuels to a gaseous stream of high purity syngas. The optimal operating conditions derived from a phase diagram analysis correspond to a certain molar flow ratio of fuel to the oxygen carrier. The co-current contact pattern ensures a high syngas purity is achieved as the gaseous species are in direct contact with the reduced state of the oxygen carrier as it exits the system. The thermodynamic phase diagram of iron–titanium oxide, as shown in Figure 1.4a, indicates the necessary ratio of oxygen carrier to fuel input flow necessary to produce >90% purity syngas. Further, Figure 1.4b indicates the addition

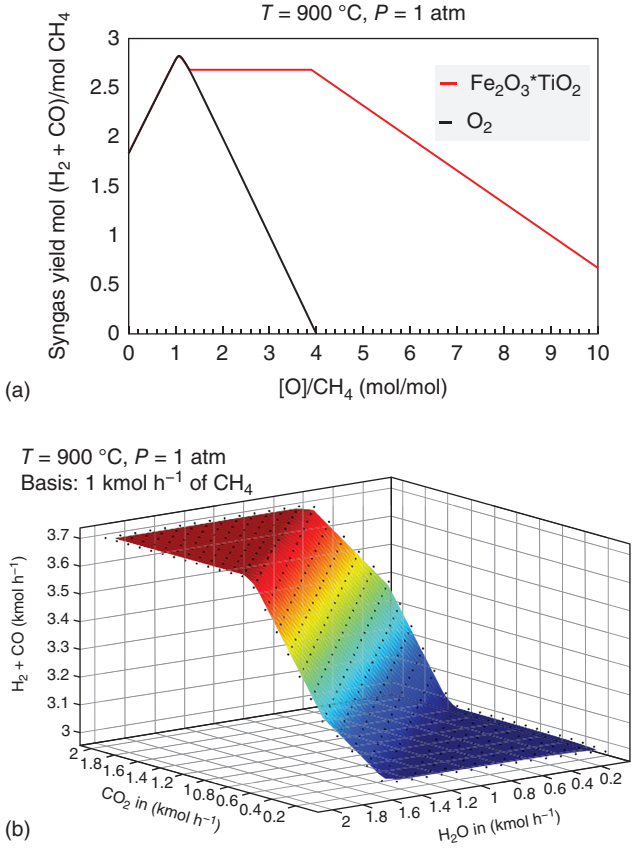

Figure 1.4 Syngas production purity at varying ratios of CH_4 and oxygen carrier flow in a co-current moving bed fuel reactor (a) and a 3-dimensional plot of the CO_2 and H_2O input and its impact on the syngas purity (b). Both results were simulated under isothermal operation conditions at 900 °C.

of steam and CO_2 can be used to adjust the ratio of CO/H_2 in the product stream while still maintaining high syngas purities.

Precise control of the oxygen carrier and gas residence time in the fuel reactor within a narrow distribution is necessary to maximize the product yield for chemical looping partial oxidation applications [23, 28, 35]. As illustrated in Figure 1.5a, fluidized bed operations are challenged with a wide residence time distribution for the solids due to the well-mixed nature of a bubbling fluidized bed. This result corresponds to wide distribution of metal oxide oxidation states in the reactor. The available lattice oxygen in the higher oxidation metal states can result in over conversion of the fuel to CO_2/H_2O, reducing the syngas selectivity. Further, the gas species exist both in the interstitial spaces emulsified with the solid media and in bubble phase generated when the superficial gas velocity exceeds the minimum fluidization velocity. Mass diffusion limitations between the bubble phase and emulsion phase can result in unconverted gaseous fuel species which can further reduce the syngas product yield. The packed moving bed is a possible design that can address these challenges. As illustrated in Figure 1.5b, the moving bed solids distribution exiting the fuel reactor is precisely controlled to a single oxygen carrier conversion value. The solids travel as a mass flow downwards and the superficial gas velocity is maintained below the minimum fluidization velocity preventing the formation of a bubble phase.

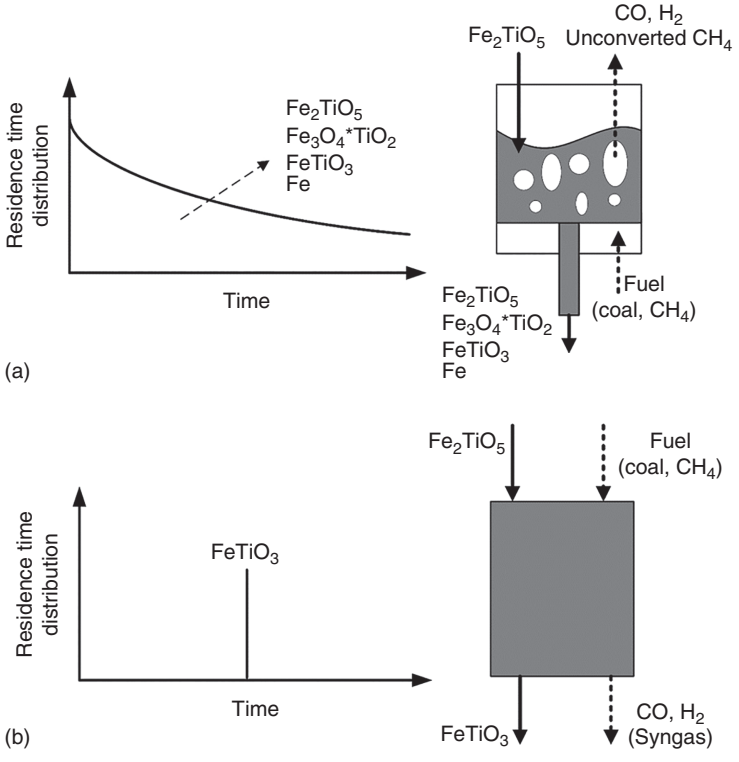

Figure 1.5 Conceptual Fe—Ti based oxygen carrier oxidation state distribution in a fluidized bed (a) and moving bed (b) fuel reactor.

As the moving bed design ensures a narrow distribution of oxygen carrier conversion along the height of the reactor, the chemical looping process design is simplified as the syngas yield from the fuel reactor is entirely thermodynamically driven. Here, reaction kinetics considerations are only necessary to supply sufficient residence time for the gas and solid phases to achieve the thermodynamically expected limits. Excessively high residence time of gaseous species will not impact the syngas yield as the gas composition at the outlet of the fuel reactor will be in equilibrium with the oxidation state of the oxygen carrier material used.

The co-current moving bed fuel reactor design is generally directed towards chemical looping processes for fuel gasification or reforming to syngas. OSU is developing the shale gas to syngas (STS) chemical looping reforming process and coal to syngas (CTS) chemical looping gasification processes. Both processes are completing sub-pilot demonstrations at the 15 and 10 kW_{th} capacities. Each process will be presented in Section 1.5.

1.3 Chemical Looping Reactor System Design Considerations for Moving Bed Fuel Reactors

As shown in Figure 1.1, the moving bed fuel reactor system comprises two or more reactors operated in moving bed and fluidized bed modes, respectively, for fuel conversion (fuel reactor) and oxygen carrier particle regeneration (air reactor). The reactors are connected using nonmechanical gas sealing devices and a gas–solid separator. The fuel reactor can be operated in counter-current or co-current moving bed mode, where the solid oxygen carrier particles travel downwards by gravity while the process gases flow upwards or downwards. The air reactor is a fluidized bed reactor which uses air for fluidization and regeneration. The air reactor is connected to a pneumatic riser to transport the oxygen carriers back to the fuel reactor with oxygen-depleted air from air reactor [36–38].

Design and sizing of the reactors and interconnecting gas-sealing devices are based on hydrodynamic calculations. The range of operating conditions, including temperature, fuel capacity, and residence times of gas and solid in each of the reactors, must also be identified for purpose of system design calculations. Based on the operating conditions, a performance model of the system can estimate the expected chemical reactions and process gas composition, and the gas flow rate in each of the reactors can be determined.

1.3.1 Mass Balance and Solids Circulation Rate

For a continuous steady-state operation of the chemical looping system, the amount of oxygen consumed by the fuel in the fuel reactor is the amount of the oxygen supplied by the oxygen carrier particles circulating in the system. The oxygen carried by the oxygen carrier particles is obtained from the air in the air reactor. It is essential for the chemical looping system to achieve a certain solids circulation rate so as to maintain the mass balance of the system. If the solids circulation rate is insufficient, the available lattice oxygen provided in the

oxygen carrier particles will be incapable of performing the desired chemical reactions in the fuel reactor – i.e. the fuel will not be fully converted and/or utilized. If the solids circulation rate is too large, the sizes of the reactors and other auxiliary devices need to be designed unnecessarily larger, which increases the operational cost. For the gasification system, which is very sensitive to the oxygen carrier-to-fuel ratio, a higher than demand oxygen carrier particle circulation rate will reduce the fuel selectivity to syngas in the fuel reactor, and in turn lower the quality of syngas yield.

The amount of solids circulation rate of a chemical looping system is determined by the fuel processing capacity of the system, the desired composition of the product gas, and the material of the oxygen carrier particles and their properties such as the degree of reduction and amount of support.

1.3.2 Heat Management

The chemical reactions occurring in the moving bed fuel reactor between fuel and metal oxide are normally net endothermic, while, the regeneration reaction of reduced metal oxide by O_2 in the air flow in the air is exothermic, generating heat. According to the energy balance of the system for chemical looping combustion applications, the sum of the heat for the complete set of chemical reactions of chemical looping combustion system is equal to the heat of direct combustion of fuel with air. Thus, the heat releases from the air reactor is greater than the heat consumed in the fuel reactor. The exothermic heat resulting from the metal reaction with oxygen in chemical looping combustion system is used to provide the endothermic heat requirement for the fuel reactor and to produce electricity and/or steam.

In the air reactor, due to the large amount of heat generated by the re-oxidation reaction of oxygen carrier, the adiabatic temperature rise can occur sharply and result in the melting or softening of the oxygen carriers if the excess heat produced is not properly removed. Excess air input or cold shots, inert material loading in the oxygen carrier, and/or continuous heat removal via in-bed heat exchangers are generally accepted methods to mitigate and control the air reactor temperature. The softening temperature of the oxygen carrier is the maximum possible temperature at which the air reactor in the chemical looping combustion system is operable as the softening of the oxygen carrier can result in particle agglomeration and defluidization.

Similarly, in the fuel reactor, as the net reactions are endothermic, the temperature of the particles decrease, causing the chemical reaction to slow down. The temperature at which the desired chemical reactions are kinetically unfavorable is the minimum possible temperature for the operation of the fuel reactor in the chemical looping combustion system. Further, the operating temperature of the fuel reactor affects the phase equilibrium of the metal oxide. For example, a reasonable fuel reactor temperature for chemical looping combustion system shall provide a minimum amount of CO and H_2 exiting from the fuel reactor gas outlet and a maximum oxygen release from metal oxide. Depending on the reactions under consideration, the temperature in the chemical looping reactors may vary from 400 °C to more than 1000 °C.

For efficient heat integration of a chemical looping system, it is desirable that enough heat is transported from the air reactor to the fuel reactor by oxygen carrier particles. When the temperatures of solids, fuel, and product are determined, the required solids flow rate to carry enough heat to the fuel reactor is obtained. Compared to the mass flow rate of oxygen carrier required by mass balance of the chemical reactions, the difference is the amount of inert material needed so that both the heat in the fuel reactor and the particle temperature are successfully managed. Another favorable effect of loading inert materials such as Al_2O_3, SiC, and TiO_2 is to improve the particle recyclability. The mass ratio of the inert material and the metal oxide is called the support-to-oxygen carrier mass ratio.

1.3.3 Sizing of Reactors

The sizing process of the fuel reactor normally starts with the determination of the gas velocity, which is an important parameter for the smooth operation of the fuel reactor and is bounded by is operational mode, i.e. fluidized bed and moving bed, and the hydrodynamics of the particles, i.e. the minimum fluidization velocity. For the fuel reactor operated under fluidized bed mode, the gas velocity shall be higher than the minimum fluidization velocity. It is usually several times of the minimum fluidization velocity to utilize the advantages of the fluidized bed reactors including good gas–solids contact mode, uniformity, and intensive heat transfer between gas and solids. For a moving bed reactor, however, the gas velocity shall be less than the minimum fluidized velocity to avoid the fluidization of the bed material. The relationship between the gas velocity and the minimum fluidization velocity can be expressed as,

$$u_{g_{reducer}} = k \cdot u_{mf} \tag{1.2}$$

where $k > 1$ for fluidized bed reactor and $k < 1$ for moving bed reactor.

With the determination of the gas velocity, the volume fraction of the solids in the fuel reactor can be obtained from the operational mode and the hydrodynamic characteristics of the oxygen carrier particles. The cross-sectional area of the fuel reactor can also be determined based on the amount or flow of gas process through it. The volume of the reactor can then be determined. A requirement for the volume of the fuel reactor is that it should provide sufficient residence time to achieve the thermodynamic equilibrium of the conversion of oxygen carrier particles and fuel, which gives the following criteria:

$$\frac{\alpha_s \rho_s V_r}{\dot{m}_s} \geq T_s \tag{1.3a}$$

$$\frac{(1-\alpha_s)\rho_g V_r}{\dot{m}_g} \geq T_g \tag{1.3b}$$

where V_r is the volume of the reactor; α_s is the volume fraction of the solids, which is determined by the operational state of the fuel reactor; ρ_s and ρ_g are the densities of the oxygen carrier particles and process gas; $\dot{m}_s$and $\dot{m}_g$are the solids circulation rate of the system and the mass flow rate of the process gas; T_s and T_g are the required residence time for the oxygen carrier particles and gases,

which are determined by the properties of the oxygen carrier particles and fuel, chemical reaction types, and the reactor operational conditions. The fuel reactor height is obtained from its required cross-sectional area to prevent particle fluidization and required volume to achieve the minimum gas and solid residence times.

1.3.4 Sizing of the Air Reactor

Because the regeneration reaction of reduced iron particles with air is a highly exothermic reaction in the air reactor, the generated heat has to be efficiently removed to maintain a constant reactor operating temperature and to avoid sintering and agglomeration of the oxygen carrier. Therefore, the air reactor is generally designed and operated as a fluidized bed because of its excellent gas–solids contact mode and effective heat transfer characteristics. The regenerated particles are then transported back to the fuel reactor via a lean phase pneumatic conveying riser.

The design basis for the air reactor and riser are closely dependent on each other, as the air introduced into the air reactor performs three functions: provides oxygen for oxygen carrier regeneration, fluidizes the oxygen carrier in the air reactor, and provides gas flow through the riser for the pneumatic transport of the oxygen carrier particles back to the fuel reactor. Under some cases, the amount of the air in the air reactor is adjusted to control the reactor temperature for the purpose of heat management. The required amount of oxygen consumption in the air reactor is determined by the fuel capacity and expected composition of the product gas. As the air reactor is operated under a fluidized bed, the gas velocity in it shall be higher than the minimum fluidization velocity, but less than the terminal velocity of the oxygen carrier particles. It is normally desired that the gas velocity is several times of the minimum fluidization velocity so as to operate the air reactor in a dense phase fluidized bed mode with a relatively compact reactor size. With the determination of the gas velocity, the volume fraction of the oxygen carrier particles in the air reactor and its cross-sectional area can be obtained. The volume and the height of the reactor can then be determined according to the requirement of providing sufficient residence time for the full regeneration of the oxygen carrier particles.

1.3.5 Gas Sealing

Gas sealing devices are required between the fuel and air reactors. Their role is to allow the oxygen carriers to flow through each reactor while keeping the gases in each reactor segregated. A reliable gas seal between each reactor is required for process safety and performance. A gas leakage from the air reactor to the fuel reactor or vice versa may result in the formation of an explosive mixture in the system, which poses a safety hazard. Further, an inefficient seal would cause fuel to leak into the air reactor and increase CO_2 emissions from the system thereby reducing the carbon capture efficiency or syngas yield. Also, leakage of air into the fuel reactor would result in formation of undesired products and contaminate the desired gaseous product.

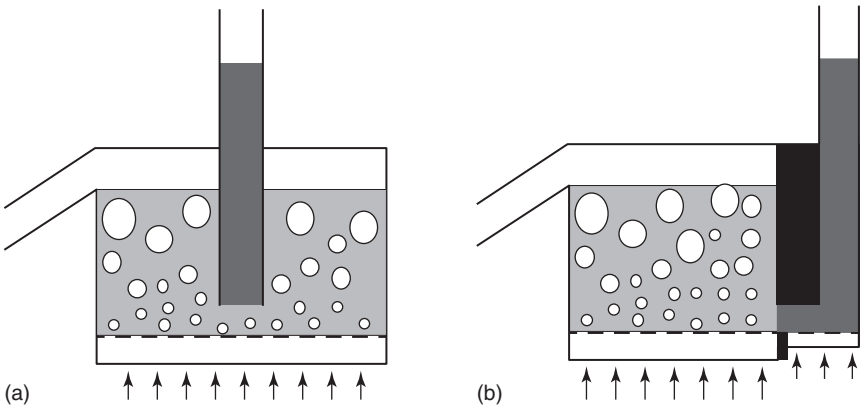

Figure 1.6 Automatic solid flow devices: (a) seal pot and (b) loop seal.

Automatic nonmechanical solid flow devices such as seal pots and loop seals, shown in Figure 1.6, are commonly used in chemical looping systems with fluidized bed fuel reactors for gas sealing purposes [38]. These nonmechanical devices are considered passive devices capable of maintaining the global solid circulation rate. However, they are generally not used for adjusting or modulating solid circulation rate in the process.

A seal pot is essentially an external fluidized bed into which the straight dip leg discharges solid particles. The solid particles and the fluidizing gas for the seal pot are discharged to the desired downstream vessel through an overflow transport line either designed as a downwardly angled pipe at the side or an overflow dip leg in the middle of the fluidized bed. With a seal pot, the solids in the dip leg rise to a height necessary to handle the pressure difference between the solids inlet and the outlet.

A loop seal is a variation of the seal pot that places the solids inlet dip leg at the side of the fluidized bed in a separate solids supply chamber. This allows for the solids return chamber to operate independently of the solids supply chamber, which results in a smaller device size, lower fluidization gas requirement, and higher efficiency. The height and the diameter of the solids supply chamber as well as its distance from the solids return chamber can be adjusted based on the process requirements necessary for balancing the pressure and handling the solids flow. Independent lubricating gas can also be added to the different locations of the solids supply chamber to assist in the operation of the loop seal.

1.3.6 Solids Circulation Control

The flow of oxygen carrier in chemical looping systems can be controlled either mechanically or non-mechanically. The use of mechanical valves to control the flow of solids was common during the early development of chemical looping processes since they allowed for maximum flexibility over the control of solids. The mechanical valves could also provide effective gas sealing between the reactors despite the pressure difference at the two ends of the valves. Although mechanical valves have been part of a number of successful tests of continuous

chemical looping processes, they have serious drawbacks. Since chemical looping processes circulate a large amount of oxygen carrier particles at high temperatures, the material of construction of the valves and their internals would have to be able to withstand the temperature. In addition, the mechanical valves must also have a high abrasion resistance due to the large flow rate of solids. In addition to the large solids flow and harsh operating conditions experienced by the mechanical valve, its repeated opening and closing during operation would accelerate the rate of wear and tear with the possibility of mechanical failure occurring during operations. The mechanical valves become cost prohibitive due to the expensive material of construction required for withstanding the operating conditions, replacement frequency that would be associated with the purchase or maintenance of large mechanical valves. Thus, it would cost intensive to scale-up the chemical looping system with mechanical valves for long-term continuous operations.

An attractive alternative to mechanical valves for solids flow control is the use of nonmechanical solids flow control devices. These devices refer to valves with no internal mechanical moving parts and that only use aeration gases in conjunction with their geometric patterns to manipulate the solid particles flow through them. The nonmechanical solids flow control devices have no moving parts and thus have no issues of wear and tear, especially under extreme operating conditions such as elevated temperatures and pressures. Also, these devices are normally inexpensive as they are constructed from ordinary pipes and fittings. Due to their simplicity, the nonmechanical solids flow control devices can be quickly fabricated avoiding the long delivery times associated with mechanical valves. They are widely used in industries due to their advantages over mechanical solids flow control devices.

The most common types of nonmechanical solids flow control devices, also called nonmechanical valves, include the L-valve and J-valve, shown in Figure 1.7a. The principles of operation for these two types of valves are the same, with the only major difference being their shape and the direction of solids discharge. Solids flow through a nonmechanical valve is driven by the drag force on the particles caused by the slip velocity between them and the aeration gas. The aeration gas is added to the bottom portion of the standpipe section

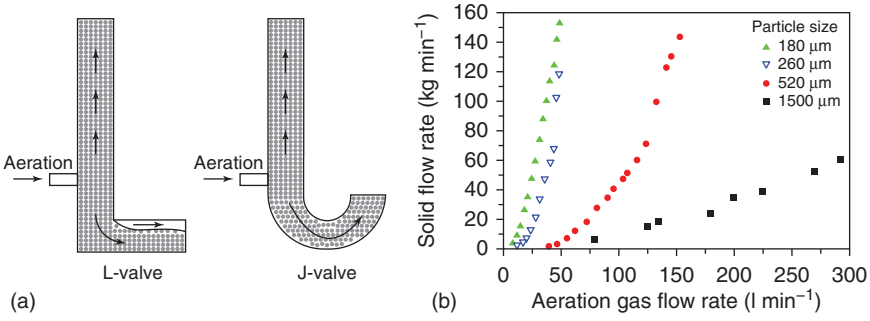

Figure 1.7 Nonmechanical L-valve and J-valve conceptual design (a) and solids flow rate as a function of aeration gas flow rate through an L-valve [36] (b).

of a nonmechanical valve and it flows downwards through the bend. The slip velocity between the gas and the solid particles produces a frictional drag force on the particles in the direction of gas flow. When the drag force exceeds the force required to overcome the resistance to solids flow around the bend, the solids begin to flow through the valve. A certain minimum amount of gas flow is required before the start of solids flow through the nonmechanical valve. Above this threshold amount of gas that is required to initiate solids flow, the solids flow rate varies proportionately to the aeration gas flow rate. A relationship between aeration gas flow rate and solids flow rate through an L-valve is shown in Figure 1.7b [36].

The actual aeration gas flow through the nonmechanical valve may be different from the amount of gas added externally through the aeration gas inlet port. It may be higher or lower than the amount of aeration gas externally injected, depending on the operating conditions of the system. In case the gas from the reactor leaks into the standpipe of a nonmechanical valve, the actual amount of aeration gas, Q_{ae}, would be the sum of the leaked gas flow into the standpipe, Q_{sp}, and the external aeration gas added from the aeration gas inlet port, Q_{ext}, as given in Eq. (1.4).

$$Q_{ae} = Q_{sp} + Q_{ext} \tag{1.4}$$

If the gas from the aeration gas inlet port leaked upward through the standpipe into the reactor, then the actual amount of aeration gas would be obtained from Eq. (1.5).

$$Q_{ae} = -Q_{sp} + Q_{ext} \tag{1.5}$$

where the negative sign in front of Q_{sp} denotes a change in the direction of aeration gas leakage compared to the previous case.

Nonmechanical valves have limitations in their operating capability based on the physical properties of the solid. Nonmechanical valves function smoothly for particles of Geldart Groups B and D but not as smoothly for particles of Geldart Groups A and C. Geldart Group A particles generally retain gas in their interstices and remain fluidized for a substantial period of time even after fluidizing gas is released from their fluidized state. Therefore, they can pass through the nonmechanical valves even after the aeration gas flow is stopped. The solids flow rate thus is not easily controlled for Geldart Group A particles. Geldart Group C particles are cohesive due to their relatively large inter-particle forces and thus are difficult to flow using aeration gas in nonmechanical valves. For a given solids flow rate, the required amount of aeration gas increases with the average particle size for solid particles of Geldart Groups B and D. This is due to the greater drag force to overcome to render the solid particles with larger diameter flow through the nonmechanical valve.

The solids flow rate pattern after the bend in the nonmechanical valve is generally in the form of pulses of relatively high frequency and short wavelength. This pulsating flow creates pressure fluctuations of a relatively steady pattern in the nonmechanical valve. The pressure drop across the valve is high when the particles stop and low when the particles surge. Increasing the length after the bend increases the solids flow rate pulses, which increases the chaotic pattern

of pressure fluctuations. The total pressure drop across the nonmechanical valve also increases with the length after the bend. In some cases, additional gas is added to the section after the bend to prevent slug formation and induce solids flow. However, this increases the total amount of external gas, and hence, the operating costs. Based on the above issues with a longer pipe length after the bend, it can be noted that the horizontal section of the nonmechanical valve should be as short as possible to minimize the pressure fluctuations and the amount of aeration gas.

1.3.7 Process Pressure Balance

A good indication and reference on the good gas sealing and proper operation of the chemical looping system is the pressure balance of the system. The pressure drops through different sections/devices of the chemical looping system reflect the gas–solids contacting modes and solids fluidization conditions at different locations of the system.

An example of pressure profile in a chemical looping system is shown in Figure 1.8. The pressure drop through the riser, ΔP_{riser}, represented by the line P_H–P_A in the figure indicating a smooth and slight drop of the pressure gradient from the bottom to the top of the riser, where the solids volume fraction, α_s, is commonly less than 1%. Line P_G–P_H illustrates the pressure drop in the air reactor. The air reactor is normally a dense phase fluidized bed where the pressure drop equals to the solids holdup in the bed and is much larger than that in the riser. Line P_A–P_B–P_C describes the pressure profile across the gas seal between the cyclone and the fuel reactor. There is a point with a pressure

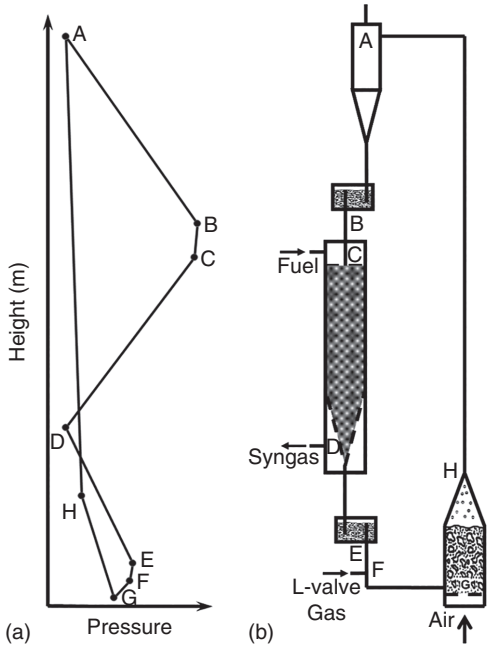

Figure 1.8 Two reactor chemical looping system with moving bed fuel reactor (b) and its pressure profile (a).

(P_B) relatively higher than the both ends of the gas seal so that the sealing gas can flow from the gas seal to both the upstream and downstream of the process and the gas mixing from either reactor to the other can be avoided. Line P_C–P_D illustrates the pressure drop across the fuel reactor which can be designed as a fluidized bed, a gas–solids counter-current moving bed or a gas–solids co-current moving bed. Line P_D–P_E–P_F represents the pressure profile across another gas seal which is located between the cyclone and the fuel reactor. The pressure distributions across these components form a closed loop and can be mathematically expressed as Eq. (1.6),

$$\Delta P_{\text{cyclone}} + \Delta P_{\text{seal 1}} + \Delta P_{\text{fuel reactor}} + \Delta P_{\text{seal 2}} = \Delta P_{\text{air reactor}} + \Delta P_{\text{riser}} \quad (1.6)$$

1.4 Counter-Current Moving Bed Fuel Reactor Applications in Chemical Looping Processes

Over the past 23 years, OSU has developed five chemical looping technologies to sub-pilot and pilot scale operations. The present section discusses the development of the counter-current moving bed fuel reactor systems of the SCL and CDCL processes for H_2 production and power generation with CO_2 capture, respectively [23].

1.4.1 Counter-Current Moving Bed Fuel Reactor Modeling

The counter-current moving bed reactor is designed to fully convert the fuel source to CO_2 and steam. Previous research was performed to simulate the reaction kinetics in combination with the moving bed reactor hydrodynamics to support the reactor size selection for optimum fuel conversion [39]. The oxygen carrier kinetics were simulated using an unreacting shrinking core model (USCM) with iron-oxide based oxygen carrier. The USCM constants were empirically quantified using experimental reduction rate data gathered from literature and OSU thermo-gravimetric analyzer studies. A one-dimensional moving bed fuel reactor model was then constructed and verified using 2.5 kW_{th} bench scale moving bed studies with H_2/CO as the reducing gases at steady state conditions. The reactor model matched well with experimental results and provided insight design of the reactor operating conditions and sizing. The results are shown in Figure 1.9. In the case of CO and H_2 as the reducing gas in the fuel reactor, a critical molar flow ratio of 1.4647 CO/H_2:Fe_2O_3 was observed where a plateau in solids conversion at 33% is observed in the middle section of the fuel reactor. This occurrence indicates that when the fuel to oxygen carrier approaches the critical ratio and the reactor is excessively long, the reduction of FeO to Fe is constrained. This is due to the equilibrium partial pressures of reducing gases in the middle of the fuel reactor inhibited the further reduction of the oxygen carrier. Once the oxygen carrier travels down close to the inlet of the reducing gas, the partial pressures favor the further reduction of FeO to Fe. To eliminate the formation of the plateau and to maintain high

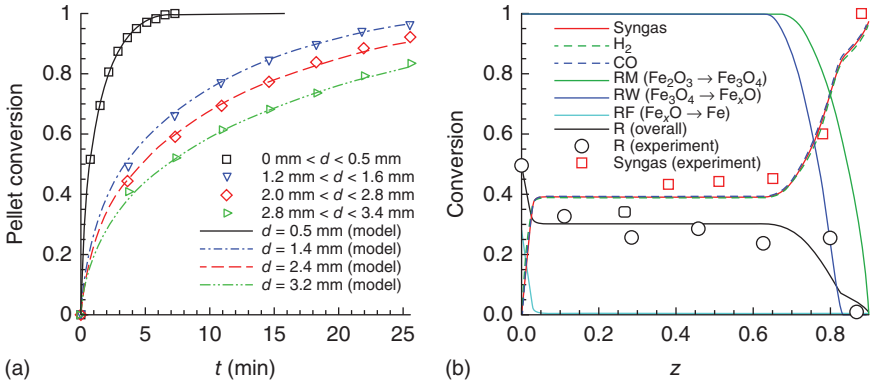

Figure 1.9 (a) Comparison between the kinetic unreacted shrinking core model and the experimental data for different Fe_2O_3 particle sizes; (b) moving bed fuel reactor model comparison with 2.5 kW_{th} bench unit test run at 1.46 CO/H_2:Fe_2O_3 molar flow ratio.

fuel conversion to CO_2, one should operate the counter-current moving bed reactor at a fuel:oxygen carrier flow ratio at a slightly lower value than the critical ratio. Parametric studies with the 25 kW_{th} sub-pilot counter-current moving bed reactor were performed to determine if the critical ratio also exists when using methane as the reducing gas in the fuel reactor. Figure 1.10 summarizes the solids profile for three test conditions with varying CH_4 to Fe_2O_3 flow ratio [40]. Here, a plateau is observed at a solid conversion of approximately 33% when the when the CH_4:Fe_2O_3 molar flow ratio is 0.466, but not observed when the ratio is decreased to 0.366. Therefore, a critical flow ratio exists for methane conversion to CO_2 between 0.366 and 0.466 similar to the model's prediction for CO conversion to CO_2. Note, the stoichiometric lattice oxygen requirement of the oxygen carrier for converting CH_4 to CO_2 and H_2O is four times greater than when CO and H_2 is used as the reducing gas.

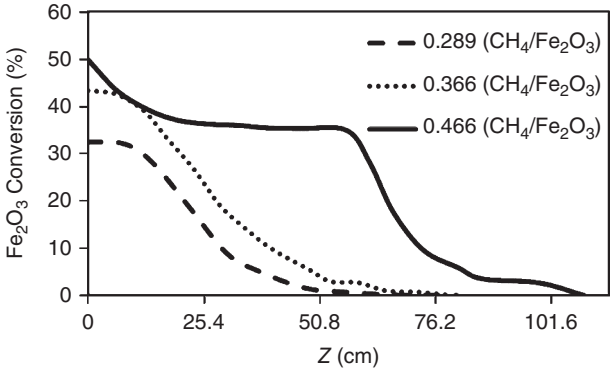

Figure 1.10 Oxygen carrier profile at steady state operation in the fuel react at varying CH_4:Fe_2O_3 molar flow ratios using a 25 kW_{th} sub-pilot chemical looping reactor system operating isothermally at 975 °C.

1.4.2 Syngas Chemical Looping Process

The SCL process, conceptually illustrated in Figure 1.1a, consists of a counter-current moving bed fuel reactor for CO_2 capture, a counter-current moving bed oxidizer for H_2 production, and a dense fluidized bed air reactor for oxygen carrier regeneration and heat production [1, 30, 40–43]. The counter-current moving bed design reduces the Fe-based oxygen carrier to Fe/FeO from the fuel reactor. The low oxidation state of the oxygen carrier entering the oxidizer is thermodynamically favored for H_2 production via the steam–iron reaction. The partially oxidized, Fe_3O_4, oxygen carriers are transported to the air reactor to be fully regenerated to Fe_2O_3 where the heat generated is used to compensate for the endothermic reactions in the fuel reactor and parasitic energy requirements of the overall processing plant.

In the case of integrated gasification combined cycle (IGCC), the SCL is considered a process intensification approach to replace the water gas shift and acid gas removal units with a single chemical looping reactor. A process flow diagram of IGCC plant incorporating the SCL reactor is illustrated in Figure 1.11. A techno-economic analysis (TEA) for IGCC–SCL power plant was performed in comparison to a conventional IGCC process with 90% CO_2 capture [44–48]. The results of TEA are summarized in Table 1.2. The SCL–IGCC system

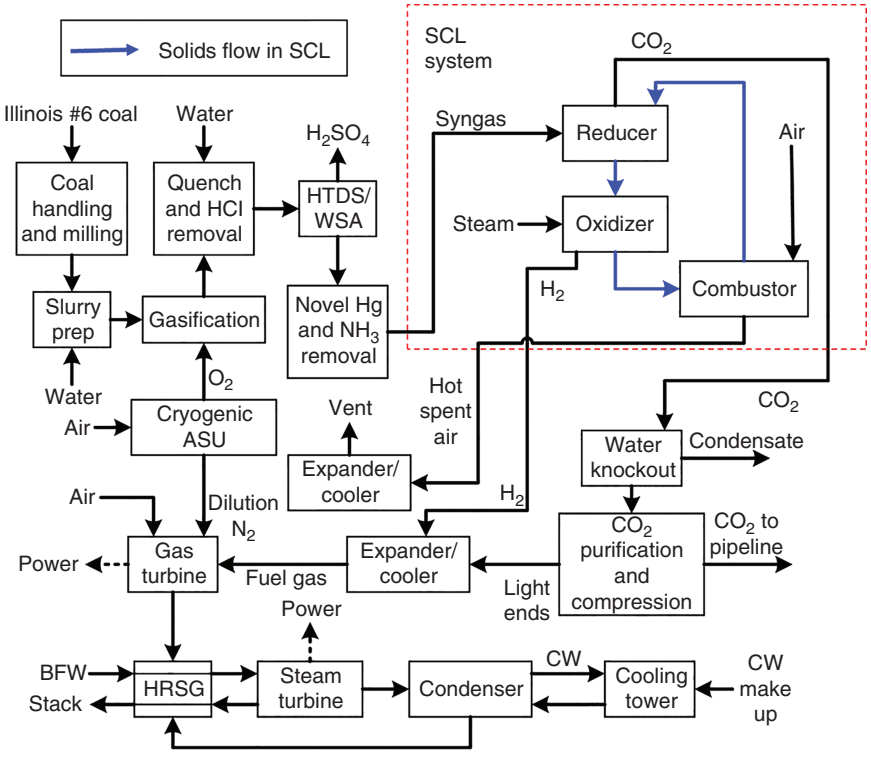

Figure 1.11 Process flow diagram of the SCL process for H_2 production integrated into an IGCC process.

Table 1.2 Economic comparison of the SCL plant for H_2 production with >90% carbon capture in an IGCC configuration.

Parameter (2011 $)	Baseline IGCC	SCL–IGCC
Total plant cost ($/kW)	3324	2934
Cost of electricity ($/MWh)	143.1	133.8

reduces the total plant costs by ~10%, resulting in a reduction in the first year cost of electricity (COE) from $143/MWh (2011 $) for the baseline case to $134/MWh (2011 $) when adopting the SCL reactor system. The case of natural gas as the feedstock, the SCL process is capable of replacing the conventional steam–methane reformer to produce high purity H_2 as an industrial gas product. The SCL's oxidizer reactor is capable of producing high purity H_2 without the need for additional gas–gas separation units, which represent nearly 75% of the capital cost in a conventional SMR process for industrial H_2 production.

Over 450 h of operation of the 25 kW_{th} SCL sub-pilot unit at the OSU clean energy research facility have been completed with smooth solids circulation and efficient reactor operation. Sample results from a continuous three-day demonstration, illustrated in Figure 1.12, indicate that nearly 100% of the simulated syngas was converted to CO_2 and H_2O in the fuel reactor with 99.99% purity H_2 produced from the oxidizer. Figure 1.13 summarizes three test conditions where the steady state fuel conversion results were compared to the theoretical expected fuel reactor performances for a counter-current moving bed and fluidized bed reactor.

A pressurized 250 kW_{th}–3 MW_{th} SCL pilot plant was constructed at the successful completion of the 25 kW_{th} sub-pilot demonstration. This pilot plant, constructed at the National Carbon Capture Center in Wilsonville, AL, represents the first large scale demonstration of a high pressure chemical looping process for high purity H_2 production. Figure 1.14a shows a picture of the constructed SCL pilot plant and Figure 1.14b shows sample results of the fuel reactor conversion

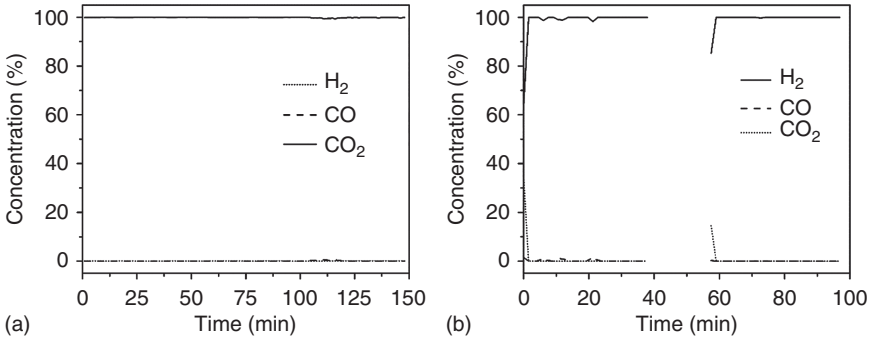

Figure 1.12 (a) Fuel reactor gas outlet composition obtained during sub-pilot scale demonstration of the SCL process; z-2. (b) Oxidizer outlet gas composition obtained during sub-pilot scale demonstration of the SCL process.

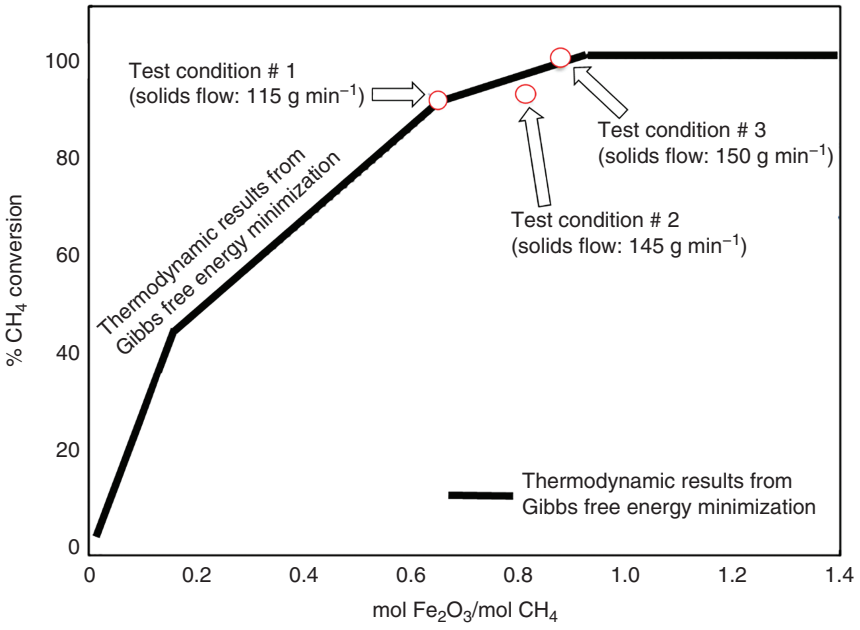

Figure 1.13 Analysis of syngas-conversion-sensitivity with respect to Fe_2O_3/syngas molar flow ratio for a fluidized bed reactor and a moving bed reactor.

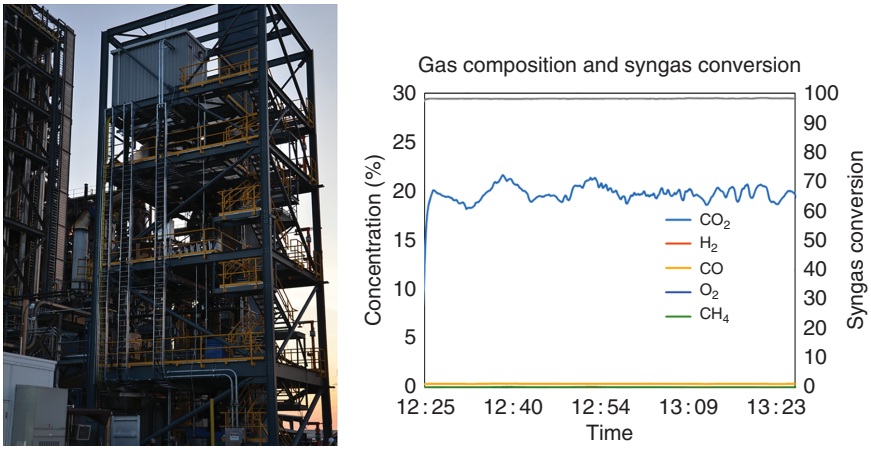

(a) (b)

Figure 1.14 Photo of 250 kW_{th}–3 MW_{th} SCL pilot plant at NCCC (a) and sample results of the fuel reactor performance (b).

profile. The demonstration results, using the syngas as feedstock from Kellogg Brown & Root (KBR's) transport gasifier, are consistent with the thermodynamic predictions from ASPEN and sub-pilot scale experiments. Further operation of the SCL pilot plant are ongoing for continuous high purity H_2 production for gasified coal.

1.4.3 Coal Direct Chemical Looping Process Development

CDCL process represents an advanced oxy-combustion technology for CO_2 capture that does not require molecular oxygen produced from air separation unit (ASU). Figure 1.3 illustrates the fuel reactor design for the CDCL process for the counter-current operation to produce high purity CO_2 while maintaining high oxygen carrier conversion. Figure 1.15a is a simplified process flow diagram for the integration of the CDCL process with a supercritical steam cycle for power generation with >90% CO_2 capture. Babcock & Wilcox Power Generation Group (B&W) in collaboration with OSU performed a TEA of the CDCL process at the 550 MW_e capacity. The reactor sizing and conceptual design of the power plant were completed (shown in Figure 1.5b) and incorporated into the fixed capital cost model. Table 1.3 summarizes the economic assessment of the CDCL process in comparison to a pulverized coal power plant without CO_2 control and a plant with an amine scrubber for post combustion CO_2 capture [49–51]. The CDCL process achieves 96.5% carbon capture efficiency with a 26.8% increase in COE compared to a conventional pulverized coal supercritical steam power plant with no CO_2 control. When compared to the 63.7% increase in COE required for post combustion CO_2 capture with amine scrubbers, the CDCL process is considered a promising approach to mitigate CO_2 emissions in power generation from fossil fuels. The major cost savings achieved in the CDCL plant is due to the simplicity of the chemical looping reactor design to achieve full fuel conversion in a single loop. Further, Figure 1.15a and Table 1.3 indicate that the capital costs of the CDCL reactor system is offset by the replacement of the pulverized coal boiler. Additional equipment requirements for the CDCL process are limited to the CO_2 conditioning stream for sulfur removal and CO_2 compression for transportation.

The CDCL process has been demonstrated at the 25 kW_{th} sub-pilot scale for over 1000 h of operation with solid fuels ranging from woody biomass to anthracite coals [32–34, 52–55]. A continuous 200-h demonstration of sub-pilot unit was completed in 2012 showing nearly 100% coal conversion to CO_2 with no carbon carryover to the air reactor. Figure 1.16 shows sample data collected on the gas composition collected from the fuel and air reactor during the 200-h demonstration.

Recent efforts have been directed to characterize the fate of sulfur species in the coal to verify the necessity of a flue gas desulfurization (FGD) device on each of the gas outlets. The tests were conducted using sub-pilot CDCL reactor system shown in Figure 1.17a. The gas sampling conditioning system used for the fuel and air reactor was designed to ensure the sulfur species was maintained in the gas phase during condensate removal. Figure 1.18 summarizes the sulfur balance between the fuel and air reactor gas outlets and the residual amount in the ash when Powder River Basin (PRB) sub-bituminous coal is used as the fuel input. The results show that <5% of the sulfur is emitted from the air reactor gas outlet which corresponds to a lower emissions rate than the Environmental Protection Agency regulation requirement of <1.4 lb sulfur/MW_{gross}. Thus, the sub-pilot CDCL operations indicate the use of a FGD unit on the flue gas stream of the air reactor is not required. The success of the 25 kW_{th} sub-pilot CDCL testing unit led to the construction of a 250 kW_{th} pilot unit. Figure 1.17b shows

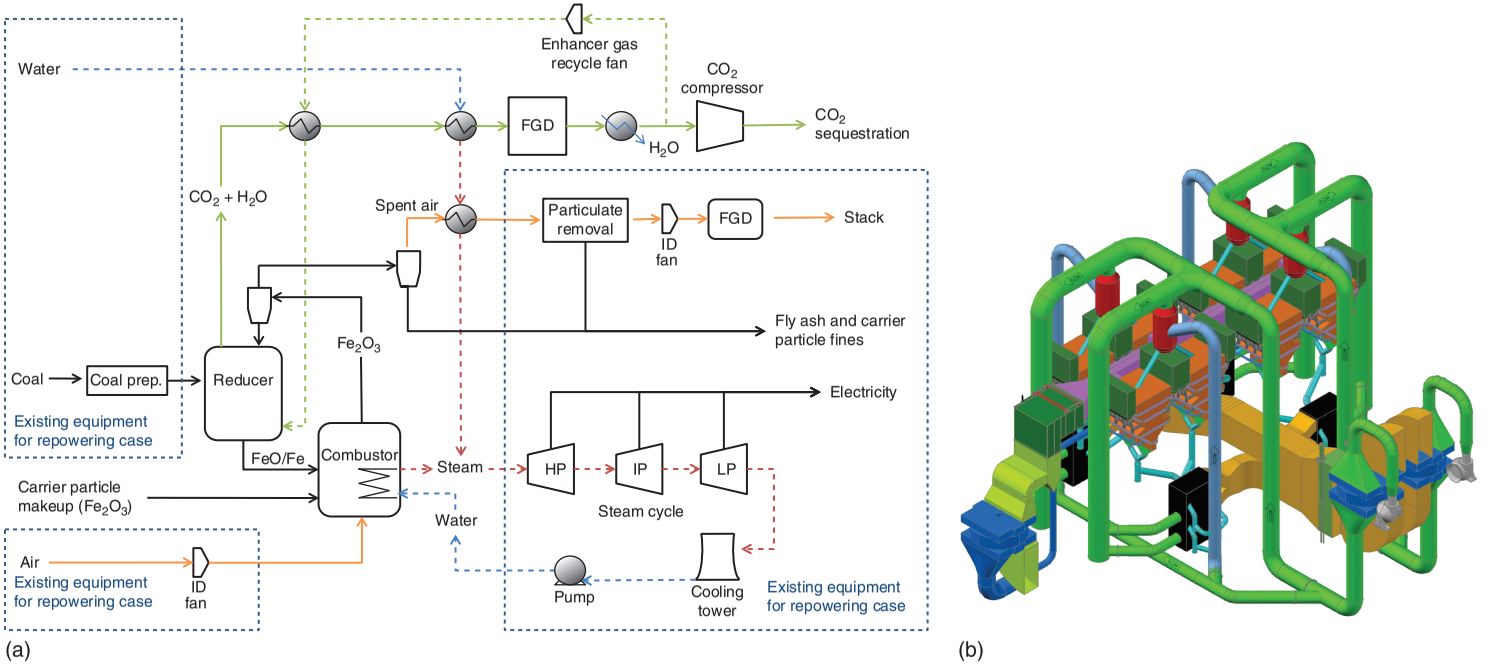

Figure 1.15 (a) Process flow diagram of CDCL process integrated a supercritical steam cycle. Items located with the blue dotted boxes indicate existing equipment in a conventional pulverized coal power plant. (b) Image of the conceptual design of a 550 MW_e CDCL plant.

Table 1.3 Comparison of the CDCL chemical looping technology for CO_2 capture with a base amine based CO_2 capture plant.

	Base plant	MEA plant	CDCL plant
Coal feed (kg h^{-1})	185 759	256 652	205 358
CO_2 capture efficiency (%)	0	90	96.5
Net power output (MW_e)	550	550	550
Net plant HHV efficiency (%)	39.3	28.5	35.6
Cost of electricity ($/MWh)	80.96	132.56	102.67
Increase in cost of electricity (%)	—	63.7	26.8

MEA, mono-ethanol-amine and HHV, high heating value.

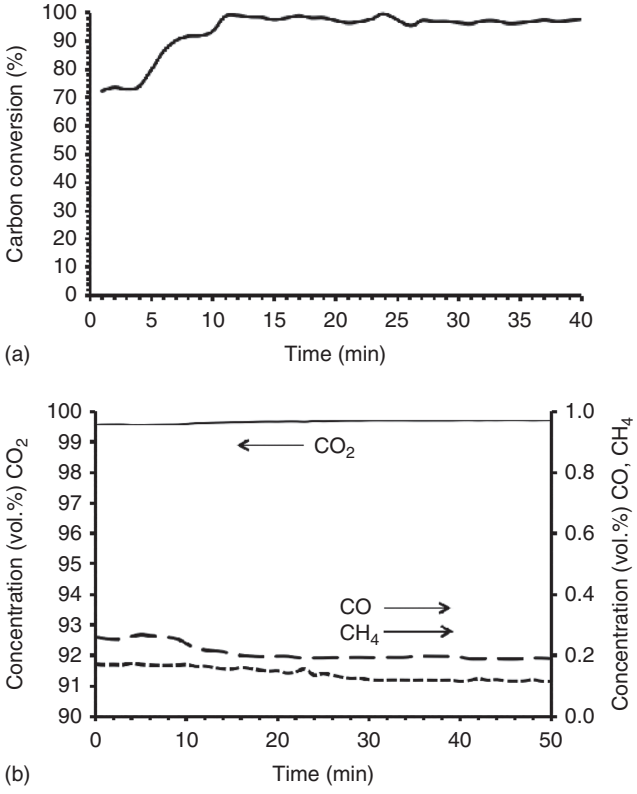

Figure 1.16 (a) Carbon conversion profile for CDCL operation, s-2; (b) fuel reactor gas outlet composition for long-term CDCL operation.

the constructed pilot unit at B&W's Research Center in Barberton, OH. The pilot unit operations will analyze the scale up factors for the coal feed distribution in the moving bed fuel reactor and the performance of the fuel reactor under adiabatic operating conditions. Construction and assembly of the unit was completed and the component and reactor commissioning activities have commenced. Unit testing with coal feed is anticipated to be completed in early 2017.

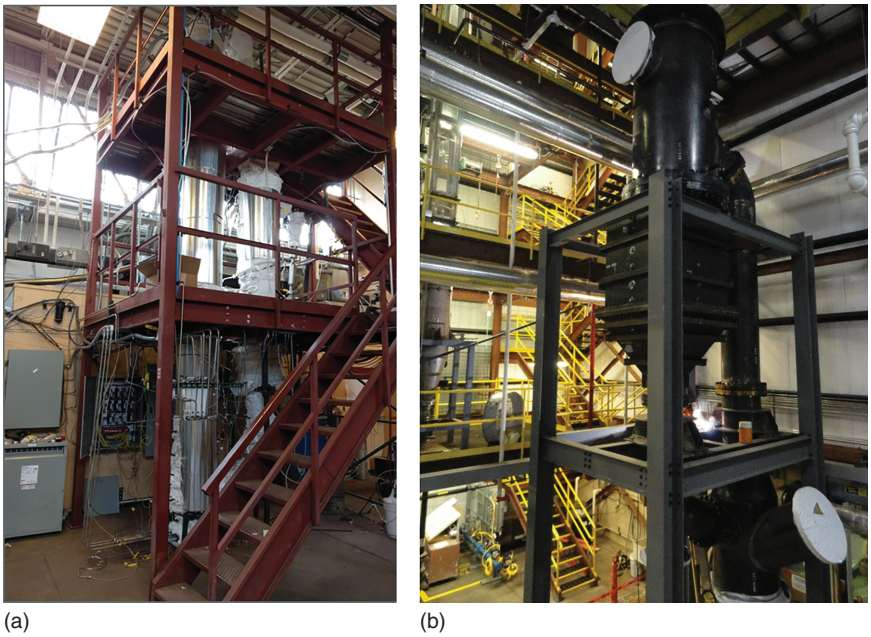

(a) (b)

Figure 1.17 Photo of the 25 kW_{th} sub-pilot CDCL unit (a) and the 250 kW_{th} CDCL pilot unit (b).

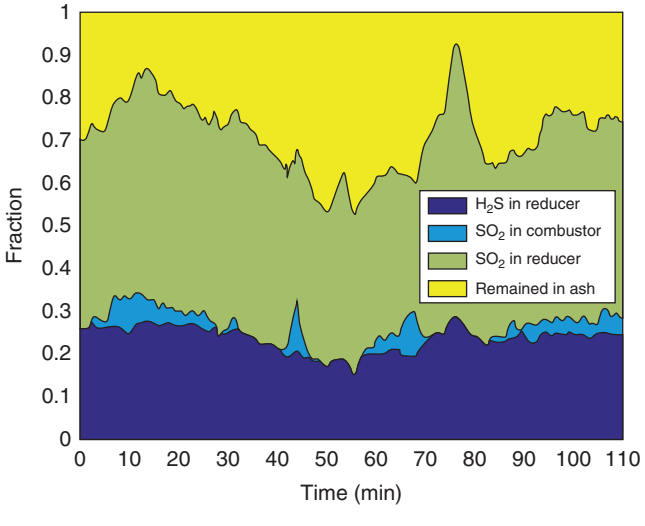

Figure 1.18 Sulfur balance in CDCL sub-pilot operation with PRB coal at 950 operating temperature.

1.5 Co-current Moving Bed Fuel Reactor Applications in Chemical Looping Processes

Co-current moving bed reactor system is directed for partial oxidation of solid and gaseous fuels to syngas. The present section describes two applications of the co-current moving bed fuel reactor for coal and natural gas conversion.

1.5.1 Coal to Syngas Chemical Looping Process

The CTS chemical looping process was developed for a high efficiency conversion of solid fuels to syngas [56]. The CTS process uses a co-current moving bed fuel reactor for producing syngas and a fluidized bed air reactor for regenerating the reduced oxygen carrier material. The CTS process produces a flexible ratio of H_2:CO syngas at >90 vol% purity, eliminating the need for molecular oxygen from an ASU and water–gas sift reactor for H_2 upgrading. A case study of this chemical looping process was performed where the CTS process was integrated with a 10 000 tonne d^{-1} methanol production plant to quantify the efficiency advantages associated with the CTS system compared to a conventional coal gasification process. The overall process flow for a coal to methanol plant, using the CTS coal gasification technology is shown in Figure 1.19. Table 1.4 summarizes the economic comparison of the CTS technology to a conventional gasification technology when integrated into a methanol production plant. As compared to the methanol synthesis plant using a conventional coal gasifier, a 28% reduction in the total plant capital cost is obtained when using the CTS technology. Further, the total coal input is reduced by ~14% due to higher carbon efficiency of the CTS process for coal gasification. The combined capital and operating cost reduction results in a 21% lower methanol required selling price than the baseline technology with 90% CO_2 capture. The CTS is also under

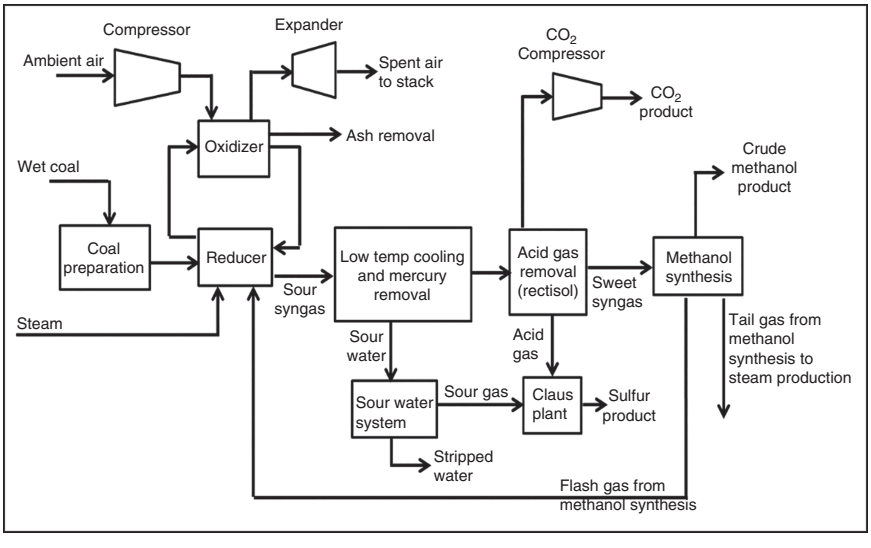

Figure 1.19 Coal to syngas process integrated in a methanol synthesis plant.

Table 1.4 Comparative summary of capital costs and cost of methanol production for the CTS case and the conventional baseline case.

Case (2011 MM$)	Baseline with 90% CO_2 capture	Baseline without CO_2 capture	CTS
CO_2 capture (%)	90	0	90
Total plant costs	4775	4568	3497
Total as spent capital	6852	6580	5003
Capital costs ($/gal)	1.23	1.18	0.89
Required selling price ($/gal)	1.78	1.64	1.41

development for power generation applications. Preliminary results have indicated that a CTS-IGCC plant can achieve the targeted regulation requirement for new coal-fired power plants of 1400 lbs CO_2/MWh_{gross} with CO_2 control equipment due to the high cold gas efficiency of the CTS process for syngas generation. This is obtained without the addition of molecular oxygen and is expected to provide significant cost savings in the electricity generation plant.

The CTS co-current moving bed concept was tested in a 2.5 kW_{th} bench-scale unit with sub-bituminous and bituminous coal over a range of operating conditions. Coal co-fed with steam and CH_4 were investigated to analyze their impact on the syngas yield and H_2:CO ratio. Representative data collected from two operating conditions for coal feed and coal and CH_4 co-feed are shown in Figure 1.20. From this figure, when only sub-bituminous coal was used as the reducing fuel in the fuel reactor, a syngas purity of ~90% was achieved – consistent with thermodynamically expected performance. A H_2:CO molar ratio of 0.65 was recorded at steady-state conditions, which was expected based on the H:C atomic ratio inherent in the coal feed. The amount of coal volatiles emitted from the fuel reactor was considered minimal due to the

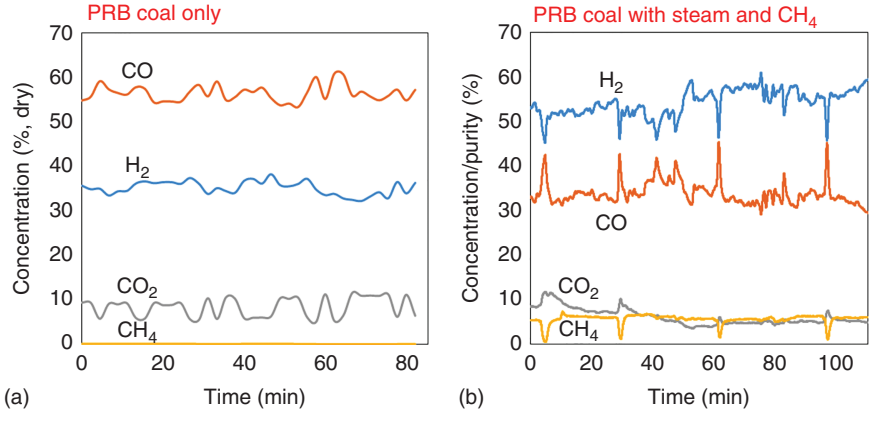

Figure 1.20 Exemplary syngas composition from CTS bench unit experiments. (a) PRB coal only. (b) PRB coal with steam and CH_4.

negligible concentrations of CH_4 observed. A carbon conversion of 93% was estimated for this test condition. Further experiments were performed for co-feeding CH_4 and/or steam to increase the ratio of H_2:CO in the syngas produced from the fuel reactor for demonstrating the versatility of the CTS technology for multiple product synthesis applications. Figure 1.20b, confirms the ratio can be adjusted by co-feeding these H_2 containing reactants. The specific test case presented in Figure 1.20b produced a syngas stream with a H_2:CO molar ratio of ~1.7, three times greater than the H_2:CO ratio produced when only coal feed is used, and with CO_2 concentrations of <10%. The results show the CTS process can adjust the H_2:CO ratio produced from the fuel reactor while maintaining a syngas purity of >90%. The versatility of the CTS process allows the process to be applicable to a range of high value chemical and fuels while eliminating the need for H_2 upgrading units such as the water–gas shift reactor and the use of molecular oxygen supplied from an ASU.

1.5.2 Methane to Syngas Chemical Looping Process

The chemical looping methane to syngas (MTS) process uses iron–titanium composite (ITCMO) materials to perform redox reactions that partially oxidize natural gas to syngas. The unique combination of a co-current downward moving bed and ITCMO particles enables the MTS process to eliminate the need for molecular oxygen, lower the temperature of operation, and significantly reduce the steam and natural gas consumption for an equivalent amount of liquid fuels production. The MTS process consists of a co-current moving bed fuel reactor integrated with a dense-phase fluidized bed air reactor to regenerate the reduced oxygen carriers. The co-current moving bed reactor operation ensures the syngas product produced achieves the thermodynamically expected performance based on the ITCMO oxygen carrier properties. The heat released from the regeneration of the oxygen carriers in the air reactor is used to compensate for the endothermic methane reforming reaction in the fuel reactor and any additional parasitic energy requirements in the overall chemical processing plant. The conditioned syngas produced from the MTS process can be used for industrial H_2 gas supply, liquid fuel synthesis, chemical production, or many other applications due the flexibility of the H_2:CO ratio produced.

Figure 1.21 illustrates the process flow diagram for the integration of the MTS process into a conventional gas to liquid (GTL) plant for the synthesis of liquid fuels at a 50 000 barrel d^{-1} production capacity. The baseline GTL plant contains an natural gas auto-thermal reformer (ATR) for syngas generation and recycles a fuel gas stream consisting mainly of light hydrocarbons (C_1–C_4). A chemical looping model was developed to compare the auto-thermal operation of the MTS process that is scaled to produce an identical amount of CO and H_2 to match the downstream liquid fuel synthesis units of the baseline comparison case. The performance results for the MTS plant using the co-current moving bed fuel reactor is summarized in Table 1.5. The metal oxide composites coupled with the co-current gas–solid contact pattern for the fuel reactor allows the MTS process to achieve a high syngas yield with less than 3% (v/v) CO_2 produced in the syngas product and a negligible carbon deposition on the oxygen carriers. Compared to

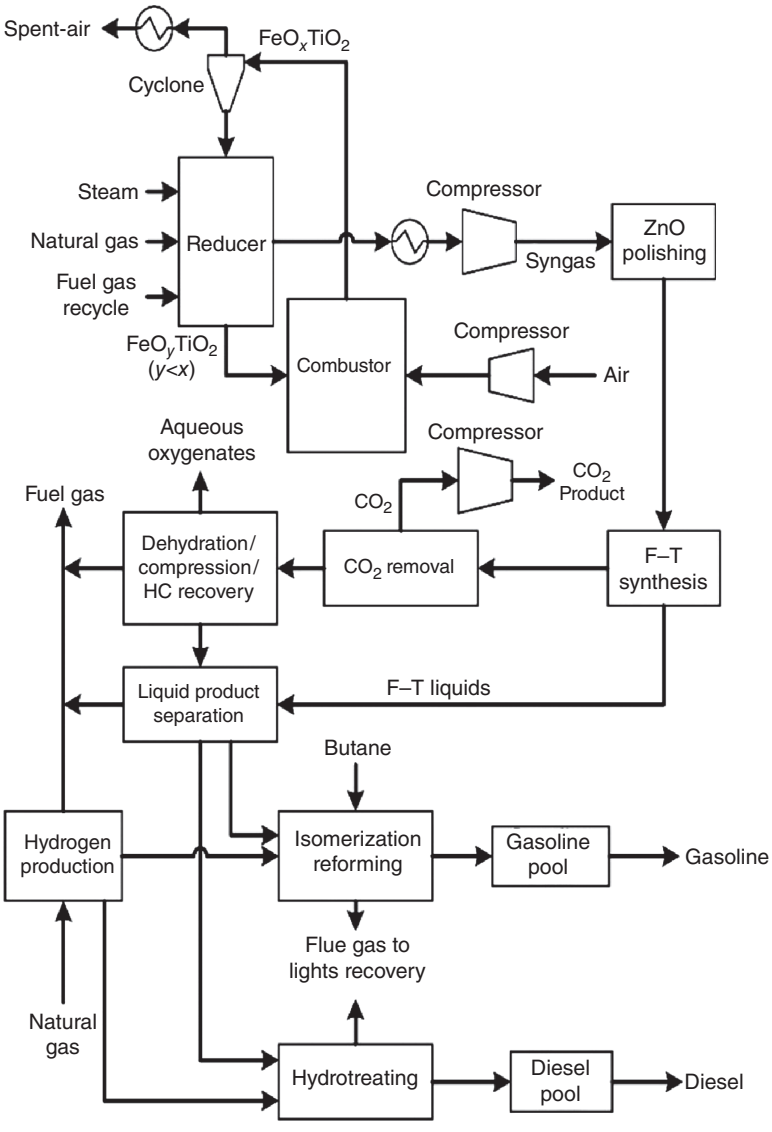

Figure 1.21 MTS process for syngas generation coupled with F–T complex for producing 50 000 bpd of liquid fuel.

conventional GTL process with ATR (utilizing 19 849 kmol h^{-1} of natural gas), the STS process requires 11% (v/v) less natural gas feed to produce an equivalent amounts of liquid fuel. Further, the MTS process eliminates the need for an energy intensive ASU. These combined benefits decrease the parasitic energy requirements of the syngas generation unit by 60% (kW_e basis). This results in twice the net power output generated from a GTL–MTS plant.

Table 1.5 Overall integrated performance of the STS process in a full-scale gas to liquids plant.

Component	Base case	MTS (10 atm)
Natural gas flow(kg h^{-1})	354 365	317 094
Natural gas flow (kmol h^{-1})	20 451	18 300
H_2O/C_{input}	0.68	0.249 9
H_2/CO	2.19	2.18
Stoichiometric number (S)	1.59	1.96
Total liquid fuel (gasoline + diesel) (bbl d^{-1})	50 003	50 003
Net plant power (kW_e)	40 800	85 000

The improved process efficiency of chemical looping system translates into an economic advantage in terms of total plant capital and operating costs. The capital cost reduction is driven by the process intensification where a single MTS reactor system can replace multiple unit operations in a conventional GTL plant, such as the ASU, the ATR for syngas generation, and the pre-reformer, into a single chemical looping unit operation. The elimination of these multiple unit operations translates to a higher capital cost savings, process thermal efficiency, and product yield. The economic analysis shows that the total plant cost for a 50 000 barrel d^{-1}y GTL plant can be reduced from ~\$86 000 barrel d^{-1} for a conventional GTL plant with ATR (2011 \$) to ~\$70 000 barrel d^{-1} (2011 \$) when incorporating the MTS chemical looping reactor system. The reduction in operating costs for the chemical looping system are mainly due to a reduction in natural gas flow. The higher methane conversion to syngas achieved by the MTS chemical looping process is due to the combination of thermodynamics of the ITCMO oxygen carrier and the co-current moving bed fuel reactor. At natural gas price of \$2/MMBtu, a MTS–GTL process will remain economically competitive even when West Texas Intermediate crude oil prices are as low as \$40/bbl.

1.5.3 CO_2 Utilization Potential

The performance estimates for the MTS shown in Table 1.5 assumed only natural gas and steam are used as the reacting gases in the fuel reactor [35, 57]. However, the quantity of syngas produced relative to the natural gas feed can be further increased by using CO_2 as a feedstock for the fuel reactor. The CO_2 reactant in combination with natural gas and steam co-feeding ensures the desired H_2:CO ratio syngas is generated for the required downstream chemical synthesis. Thus, the increase in the syngas production with CO_2 co-feed for a fuel reactor operation leads to further savings in natural gas flow beyond the 11% value shown in Table 1.5. CO_2 reaction parameter (CRP) is defined as CO_2 input to the fuel reactor divided by the CO_2 output from the fuel reactor. A CRP value of greater than 1 implies that the fuel reactor is consuming more than it is producing, acting

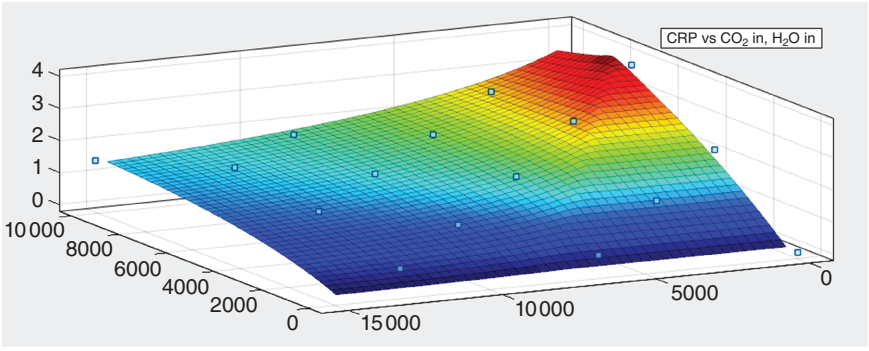

Figure 1.22 CRP variation as a function of steam molar input and CO_2 molar input at a natural gas flow of 15 300 kmol h^{-1}, Fe_2O_3:C molar ratio of 0.85, $P = 1$ atm and $T = 900$ °C.

Table 1.6 MTS system performance with CO_2 co-injection for a natural gas flow of 15 300 kmol h^{-1}, Fe_2O_3:CH_4 ratio of 0.33 and a CRP = 2.

CO_2 in (kmol h^{-1})	CO_2 out (kmol h^{-1})	CRP	H_2O (kmol h^{-1})	H_2:CO
3 500	1 748	2.00	4 800	1.89
5 000	2 488	2.01	5 600	1.80
6 500	3 246	2.0	6 300	1.72
8 000	3 990	2.05	6 800	1.64
9 500	4 742	2.0	7 200	1.57
10 000	4 992	2.0	7 300	1.54

as a net CO_2 sink. The set of conditions where CRP is greater than 1 are typically quantified by plotting CRP values as a function of CO_2 and H_2O injection flows as shown in Figure 1.22. An example of the variation of syngas production performance with varying CRP values is shown in Table 1.6.

The MTS chemical looping system with CO_2 requires only 16 000 kmol h^{-1} of natural gas for producing 50 000 bpd of liquid fuel, which translates to a reduction in the natural gas consumption of 22% over the baseline system. A 22% reduction in natural gas flow results in an annual cost saving of $60 million as compared to the baseline plant, when assuming a natural gas price of $2/MMBtu and 90% production capacity. The process performance suggests that the MTS process is a potential approach to CO_2 utilization for chemical synthesis.

1.5.4 MTS Modularization Strategy

Chemical looping processes are inherently low capital cost intensive systems due to their ability to reduce the number of unit operations to generate the desired product. Thus, researchers have engaged in designing modular chemical looping

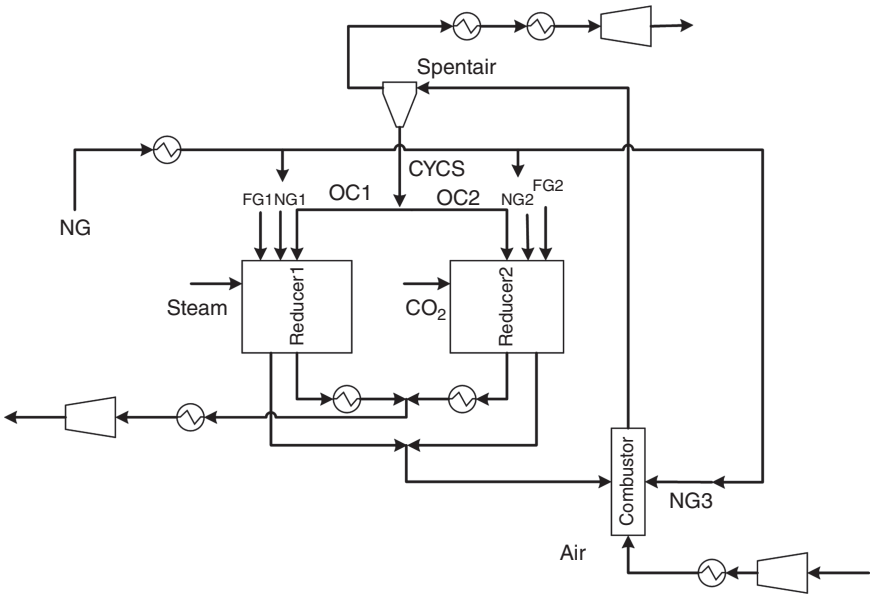

Figure 1.23 Chemical looping modular system for integration into a 50 000 bpd cobalt-based F–T process.

systems that can be cost-competitive processes even at smaller fuel processing capacities. Modular reactor designs are advantageous in increasing the operation flexibility of a chemical plant and can open opportunities for utilizing remote or stranded resources currently uneconomical to process. A modular reactor design for the MTS process suggests an increased syngas production efficiency is achieved by adjusting the fuel and reactant feed conditions in each module. Referring to Figure 1.23, the addition of CO_2 as a reactant results in a nonlinear syngas production trend from the fuel reactor, and, thus, can be exploited to maximize syngas production while maintaining the desired H_2/CO ratio [35]. The detailed material balance for the chemical looping module is shown in Table 1.7. The modularization strategy application reduces the natural gas consumption to 15 200 kmol h^{-1} for production of 50 000 barrel d^{-1} of liquid fuels.

A schematic design of the OSU 10 kW_{th} MTS fuel reactor test apparatus is given in Figure 1.24a. Multiple tests with the sub-pilot apparatus at varying CH_4: oxygen carrier flow ratios and reactant (i.e. CO_2 and H_2O) co-feed rates to verify that the experimental performance of the co-current moving bed reactor to match the thermodynamically expected syngas yields. Figure 1.24b is a sample gas profile from the co-current moving bed fuel reactor showing nearly full fuel conversion to syngas. Table 1.8 summarizes the operating conditions and results in comparison with the thermodynamic values. The results show the sub-pilot co-current moving bed fuel reactor can achieve >99% CH_4 feed conversion with 91.3% syngas purity and a CO:H_2 ratio of 1.89. Table 1.8 shows the experimental results match well with the thermodynamically expected syngas yield.

Table 1.7 Material balance for the two-reactor modular chemical looping system shown in Figure 1.23.

	Air	CO_2	CYCS	FG1	FG2	NG1	NG2	NG3	OC1	OC2	Spent air	Steam	Syngas
Temperature (°C)	900	900	1 150	900	900	900	900	900	1 150	1 150	1 150	900	755
Pressure (atm)	1	1	1	1	1	1	1	1	1	1	1	1	1
All flows (kmol h^{-1})													
Total flow	30 549	7 800	89 500	16 293	6 983	10 123	4 408	669	62 650	26 850	26 263	16 800	94 835
CH4	0	0	0	520	223	9 425	4 104	623	0	0	0	0	359
H2O	0	0	0	21	9	0	0	0	0	0	1 342	16 800	11 786
CO	0	0	0	2 248	964	0	0	0	0	0	0	0	20 720
CO2	0	7 800	0	161	69	101	44	7	0	0	697	0	6 918
H2	0	0	0	6 602	2 829	0	0	0	0	0	0	0	45 491
Fe2O3	0	0	9 948	0	0	0	0	0	6 964	2 984	0	0	0
N2	24 134	0	0	6 528	2 798	162	71	11	0	0	24 143	0	9 556
O2	6 415	0	0	0	0	0	0	0	0	0	79	0	0
n-C4H10	0	0	0	11	5	40	18	3	0	0	0	0	0
TiO2	0	0	79 552	0	0	0	0	0	55 686	23 866	0	0	0
FeTiO3	0	0	0	0	0	0	0	0	0	0	0	0	0

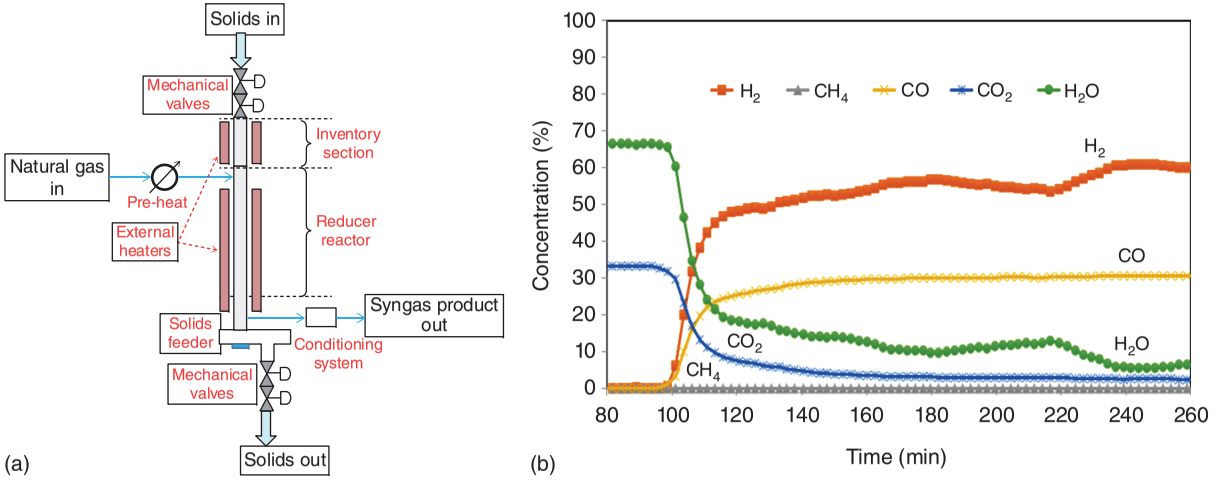

Figure 1.24 (a) Schematic of 10 kW_{th} co-current moving bed fuel reactor test unit and (b) fuel reactor gas outlet composition profile during demonstration of the 10 kW_{th} fuel reactor.

Table 1.8 Key experiment and simulated performance data of 10 kW_{th} sub-pilot STS reactor.

	Experimental results	Theoretical limit
[O]:CH_4	2.2	
Temperature (°C)	975	
CH_4 conversion (%)	>99.9	99.96
H_2:CO	1.89	1.91
CO:CO_2	11.8	12.2

1.6 Concluding Remarks

Moving bed fuel reactors are used in chemical looping processes as advanced energy conversion systems. The packed moving bed fuel reactor can be operated in the co-current and counter-current modes with respect to the gas–solid contact pattern. A counter-current moving bed fuel reactor is advantageous for full fuel conversion to CO_2 and H_2O while maximizing oxygen utilization of the oxygen carrier. The co-current moving bed fuel reactor is used for the partial oxidation of carbonaceous fuels to syngas where the precise control of the solid and gas residence times ensures the thermodynamic limits of the syngas purity and ratio produced can be achieved. Design considerations for sizing the moving bed fuel reactor and dense fluidized bed air reactor with respect to fuel process capacity, operating temperature, and oxygen carrier properties were discussed. Consideration was also provided for types of gas-sealing and solid flow control valves for integrated the operation of fuel and air reactors. The SCL and CDCL processes are exemplary chemical looping processes that use count-current moving bed fuel reactors. The CDCL process is an advanced oxy-combustion process for power generation capable of exceeding 90% CO_2 capture with minimal increase in COE (~26.8% compared to base pulverized coal power plant without CO_2 capture). Sub-pilot demonstrations confirm that nearly 100% CO_2 capture can be achieved and sulfur emissions from the air reactor are below the Environmental Protection Agency (EPA) emissions limit. The SCL has been scaled to a high pressure 250 kW_{th}–3 MW_{th} pilot plant and demonstrated for high purity H_2 production with CO_2 capture from gaseous fuels such as gasified coal syngas. The CTS and MTS process represent exemplary co-current moving bed fuel reactor chemical looping processes for the partial oxidation of solid and gaseous fuels, respectively, to syngas. Experimental studies at bench and 10 kW_{th} sub-pilot scale show the co-current moving bed fuel reactor design is capable of achieving product syngas purity and H_2/CO ratios at the thermodynamically predicted limits. When CO_2 is used as the feedstock to the co-current moving bed fuel reactor, the amount syngas produced can be increased substantially. A nonlinear relationship between the syngas produced relative to the CO_2 input can be exploited in a modular chemical looping reactor system design to substantially reduce the amount of natural gas consumed to produce an equivalent amount of syngas – over 25%

reduction in natural gas consumption compared to conventional ATR of natural gas. Thus, the simplicity of the moving bed fuel reactor design combined with its versatility and efficiency show this design is a viable approach chemical looping processes as proven by the experimental and modeling results.

References

1 Fan, L.-S. (2011). *Chemical Looping Systems for Fossil Energy Conversions*. Wiley.
2 Knoche, K. and Richter, H. (1968). Improvement of reversibility of combustion processes. *Brennstoff-Warme-Kraft* 20 (5): 205.
3 Richter, H.J. and Knoche, K.F. (1983). Reversibility of combustion processes. In: *Efficiency and Costing*, vol. 235, 71–85. American Chemical Society. doi: 10.1021/bk-1983-0235.ch003.
4 Ishida, M., Zheng, D., and Akehata, T. (1987). Evaluation of a chemical-looping-combustion power-generation system by graphic exergy analysis. *Energy* 12 (2): 147–154.
5 Bergmann, F.J. (1897). Process for the production of calcium carbide in blast furnaces. German Patent 29,384.
6 Hurst, S. (1939). Production of hydrogen by the steam–iron method. *J. Am. Oil Chem. Soc.* 16 (2): 29–35.
7 Gasior, S., Forney, A., Field, J. et al. (1961). *Production of Synthesis Gas and H_2 by the Steam–Iron Process*. Washington, DC: U.S. Department of the Interior, Bureau of Mines.
8 Lewis, W.K. and Gilliland, E.R. (1954). Production of pure carbon dioxide. US Patent 2,665,972.
9 Dobbyn, R., Ondik, H., Willard, W. et al. (1978). Evaluation of the Performance of Materials and Components Used in the CO_2 Acceptor Process Gasification Pilot Plant. Final Report. *DOE-ET-10253-T1*. Washington, DC: U.S. Department of Energy.
10 Teed, P.L. (1919). *The Chemistry and Manufacture of H_2*. Longmans, Green and Company.
11 Institute of Gas Technology (1979). Coal Gasification. *EF-77-C-01-2435*. Washington, DC: U.S. Department of Energy.
12 Lane, H. (1913). Process for the production of hydrogen. US Patent 1,078,686.
13 Institute of Gas Technology (1979). Development of the Steam–Iron Process for Hydrogen Production. *EF-77-C-01-2435*. Washington, DC: U.S. Department of Energy.
14 Otsuka, K., Wang, Y., Sunada, E., and Yamanaka, I. (1998). Direct partial oxidation of methane to synthesis gas by cerium oxide. *J. Catal.* 175 (2): 152–160.
15 Dudukovic, M.P. (2009). Frontiers in reactor engineering. *Science* 325 (5941): 698–701.
16 Nakamura, T. (1977). Hydrogen production from water utilizing solar heat at high temperatures. *Sol. Energy* 19 (5): 467–475.

17 Steinfeld, A. and Palumbo, R. (2001). Solar thermochemical process technology. In: *Encyclopedia of Physical Science and Technology*, vol. 15 (ed. R.A. Meyers), 237–256. Academic Press.

18 Jones, C.A., Leonard, J.J., and Sofranko, J.A. (1987). Fuels for the future: remote gas conversion. *Energy Fuels* 1 (1): 12–16.

19 Jones, C.A., Leonard, J.J., and Sofranko, J.A. (1987). The oxidative conversion of methane to higher hydrocarbons over alkali-promoted $MnSiO_2$. *J. Catal.* 103 (2): 311–319.

20 Steinfeld, A., Kuhn, P., and Karni, J. (1993). High-temperature solar thermochemistry: production of iron and synthesis gas by Fe_3O_4-reduction with methane. *Energy* 18 (3): 239–249.

21 Steinfeld, A. (2005). Solar thermochemical production of hydrogen – a review. *Sol. Energy* 78 (5): 603–615.

22 Adanez, J., Abad, A., Garcia-Labiano, F. et al. (2012). Progress in chemical-looping combustion and reforming technologies. *Prog. Energy Combust. Sci.* 38 (2): 215–282.

23 Fan, L.-S., Zeng, L., and Luo, S. (2015). Chemical-looping technology platform. *AIChE J.* 61 (1): 2–22.

24 Hamers, H., Gallucci, F., Cobden, P. et al. (2013). A novel reactor configuration for packed bed chemical-looping combustion of syngas. *Int. J. Greenhouse Gas Control* 16: 1–12.

25 Ortiz, M., Gallucci, F., Snijkers, F. et al. (2014). Development and testing of ilmenite granules for packed bed chemical-looping combustion. *Chem. Eng. J.* 245: 228–240.

26 Hamers, H.P., Romano, M.C., Spallina, V. et al. (2015). Energy analysis of two stage packed-bed chemical looping combustion configurations for integrated gasification combined cycles. *Energy* 85: 489–502.

27 Noorman, S. and van Kuipers, S.A. (2007). Packed bed reactor technology for chemical-looping combustion. *Ind. Eng. Chem. Res.* 46 (12): 4212–4220.

28 Luo, S., Zeng, L., Xu, D. et al. (2014). Shale gas-to-syngas chemical looping process for stable shale gas conversion to high purity syngas with a H_2:CO ratio of 2:1. *Energy Environ. Sci.* 7 (12): 4104–4117.

29 Tong, A., Bayham, S., Kathe, M.V. et al. (2014). Iron-based syngas chemical looping process and coal-direct chemical looping process development at Ohio State University. *Appl. Energy* 113: 1836–1845.

30 Li, F., Zeng, L., Velazquez-Vargas, L.G. et al. (2010). Syngas chemical looping gasification process: bench-scale studies and reactor simulations. *AIChE J.* 56 (8): 2186–2199.

31 Kathe, M.V., Empfield, A., Na, J. et al. (2016). Hydrogen production from natural gas using an iron-based chemical looping technology: thermodynamic simulations and process system analysis. *Appl. Energy* 165: 183–201.

32 Kim, H., Wang, D., Zeng, L. et al. (2013). Coal direct chemical looping combustion process: design and operation of a 25-kW_{th} sub-pilot unit. *Fuel* 108 (0): 370–384.

33 Bayham, S., McGiveron, O., Tong, A. et al. (2015). Parametric and dynamic studies of an iron-based 25-kW_{th} coal direct chemical looping unit using sub-bituminous coal. *Appl. Energy* 145: 354–363.

34 Bayham, S.C., Kim, H.R., Wang, D. et al. (2013). Iron-based coal direct chemical looping combustion process: 200-h continuous operation of a 25-kW_{th} subpilot unit. *Energy Fuels* 27 (3): 1347–1356.

35 Kathe, M., Empfield, A.M., Sandvik, P.O. et al. (2017). Utilization of CO_2 as a partial substitute for methane feedstock in chemical looping methane–steam redox processes for syngas production. *Energy Environ. Sci.* 10 (6): 1345–1349. doi: 10.1039/C6EE03701A.

36 Wang, D. and Fan, L.-S. (2015). L-valve behavior in circulating fluidized beds at high temperatures for group D particles. *Ind. Eng. Chem. Res.* 54 (16): 4468–4473.

37 Wang, D. and Fan, L.-S. (2014). Bulk coarse particle arching phenomena in a moving bed with fine particle presence. *AIChE J.* 60 (3): 881–892.

38 Knowlton, T.M. (1997). Standpipes and return systems. In: *Circulating Fluidized Beds* (ed. J.R. Grace, A.A. Avidan and T.M. Knowlton), 214–260. Dordrecht: Springer.

39 Zhou, Q., Zeng, L., and Fan, L.-S. (2013). Syngas chemical looping process: dynamic modeling of a moving-bed reducer. *AIChE J.* 59 (9): 3432–3443.

40 Tong, A., Zeng, L., Kathe, M.V. et al. (2013). Application of the moving-bed chemical looping process for high methane conversion. *Energy Fuels* 27 (8): 4119–4128.

41 Sridhar, D., Tong, A., Kim, H. et al. (2012). Syngas chemical looping process: design and construction of a 25 kW_{th} subpilot unit. *Energy Fuels* 26 (4): 2292–2302.

42 Tong, A., Sridhar, D., Sun, Z. et al. (2013). Continuous high purity hydrogen generation from a syngas chemical looping 25 kWth sub-pilot unit with 100% carbon capture. *Fuel* 103: 495–505.

43 Zeng, L., Tong, A., Kathe, M. et al. (2015). Iron oxide looping for natural gas conversion in a countercurrent moving bed reactor. *Appl. Energy* 157: 338–347.

44 Gerdes, K., Summers, W., and Wimer, J. (2011). Cost Estimation Methodology for NETL Assessments of Power Plant Performance. *Final Rep. DOE/NETL-2011/1455*. Washington, DC: U.S. Department of Energy.

45 Zoelle, A., Turner, M.J., and Chou, V. (2015). Quality Guidelines for Energy System Studies: Performing a Techno-Economic Analysis for Power Generation Plants. *DOE/NETL-2015/1726*. Washington, DC: U.S. Department of Energy.

46 Woods, M. and Matuszewski, M. (2012). Quality Guideline for Energy System Studies: Specifications for Selected Feedstocks. *DOE/NETL-341/011812*. Washington, DC: U.S. Department of Energy.

47 Turner, M.J. and Pinkerton, L. (2013). Quality Guidelines for Energy System Studies: Capital Cost Scaling Methodology. *DOE/NETL-341/0131113*. Washington, DC: U.S. Department of Energy.

48 Grant, T., Morgan, D., and Gerdes, K. (2013). Quality Guidelines for Energy System Studies: Carbon Dioxide Transport and Storage Costs in NETL Studies. *DOE/NETL-2013/1614*. Washington, DC: U.S. Department of Energy.

49 Li, F. and Fan, L.-S. (2008). Clean coal conversion processes – progress and challenges. *Energy Environ. Sci.* 1 (2): 248–267.

50 Fan, L.-S. and Li, F. (2010). Chemical looping technology and its fossil energy conversion applications. *Ind. Eng. Chem. Res.* 49 (21): 10200–10211.

51 Zeng, L., He, F., Li, F., and Fan, L.-S. (2012). Coal-direct chemical looping gasification for hydrogen production: reactor modeling and process simulation. *Energy Fuels* 26 (6): 3680–3690.

52 Luo, S., Li, J., Zhang, R. et al. (2015). Status and perspective of solid-fueled chemical looping technology. *Shiyou Xuebao, Shiyou Jiagong/Acta Petrolei Sinica (Petroleum Processing Section)* 31 (2): 426–435.

53 Zeng, L., Kathe, M.V., Chung, E.Y., and Fan, L.-S. (2012). Some remarks on direct solid fuel combustion using chemical looping processes. *Curr. Opin. Chem. Eng.* 1 (3): 290–295.

54 Li, F., Zeng, L., and Fan, L.-S. (2010). Biomass direct chemical looping process: process simulation. *Fuel* 89 (12): 3773–3784.

55 Kobayashi, N. and Fan, L.-S. (2011). Biomass direct chemical looping process: a perspective. *Biomass Bioenergy* 35 (3): 1252–1262.

56 Kathe, M.V., Xu, D., Hsieh, T.-L. et al. (2014). Chemical Looping Gasification for Hydrogen Enhanced Syngas Production with In-Situ CO_2 Capture. *Tech. Rep. OSTI: 1185194*. Washington, DC: U.S. Department of Energy.

57 Kathe, M., Fryer, C., Sandvik, P. et al. (2017). Modularization strategy for syngas generation in chemical looping methane reforming systems with CO_2 as feedstock. *AIChE J.* 63 (8): 3343–3360. doi: 10.1002/aic.15692.